Electronic Supplementary Material (ESI) for Photochemical & Photobiological Sciences.
This journal is © The Royal Society of Chemistry and Owner Societies 2019

Supporting Information for

(1,3)Pyrenophanes containing crown ether moieties as fluorescence sensors for metal and ammonium ions

Hajime Maeda,* Keigo Nakamura, Taniyuki Furuyama and Masahito Segi

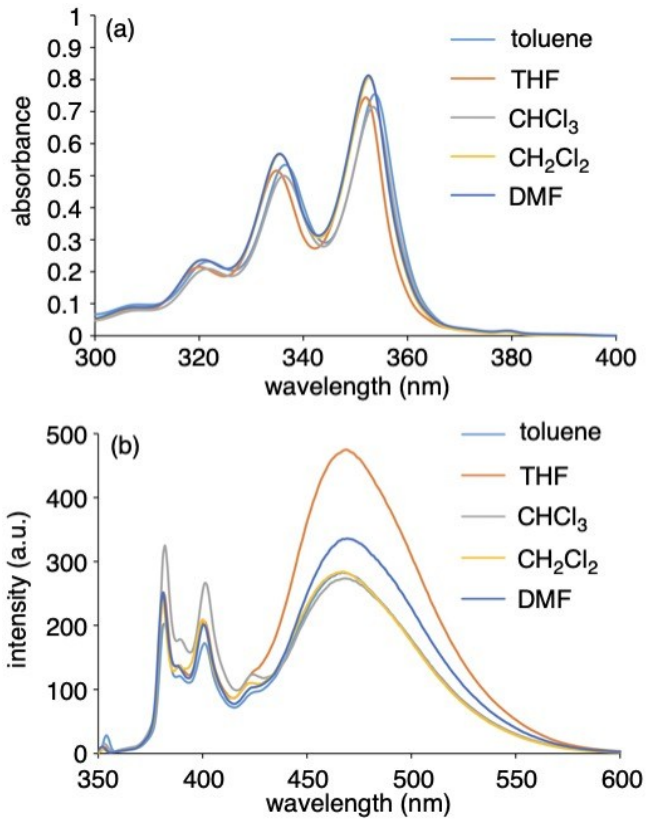

Fig. S1 (a) UV-vis absorption and (b) fluorescence spectra of **1**, 1.0×10^{-5} M, λ_{ex} = 352 (in THF and DMF), 353 (in $CHCl_3$ and CH_2Cl_2), and 354 (in toluene) nm.

Table S1 Effect of solvents on ratio of intramolecular excimer/monomer emissions of **1**.

solvent	$E_T(30)^a$	I_{460}/I_{380} [b]
toluene	33.9	1.66
THF	37.4	1.23
$CHCl_3$	39.1	1.09
CH_2Cl_2	40.7	2.09
DMF	43.2	1.36

[a] Data from C. Reichardt, Solvatochromic Dyes as Solvent Polarity Indicators, *Chem. Rev.* 1994, **94**, 2319-2358. [b] Ratio of fluorescence intensity at 460 nm (I_{460}) to that at 380 nm (I_{380}).

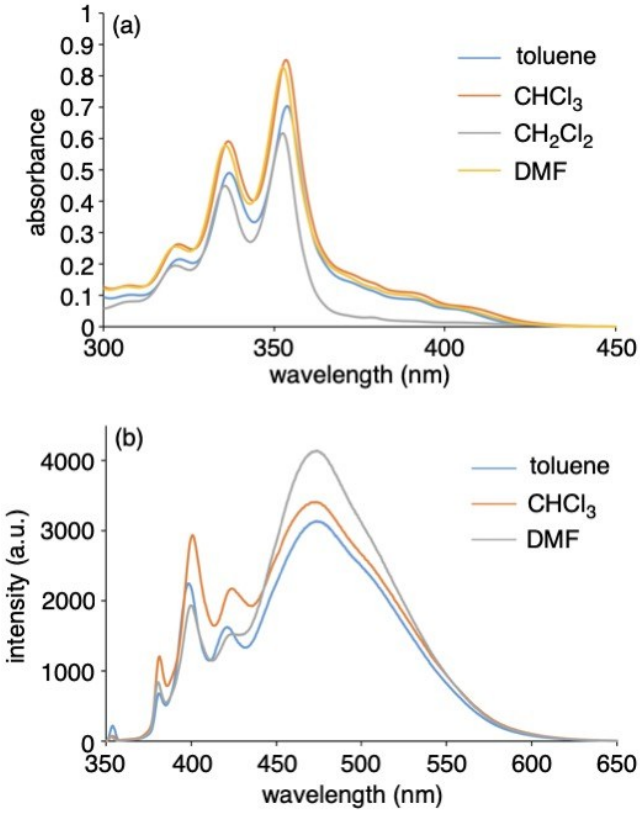

Fig. S2 (a) UV-vis absorption and (b) fluorescence spectra of **2**, 1.0 × 10^{-5} M, λ_{ex} = 352 (in DMF) and 354 (in toluene and $CHCl_3$) nm.

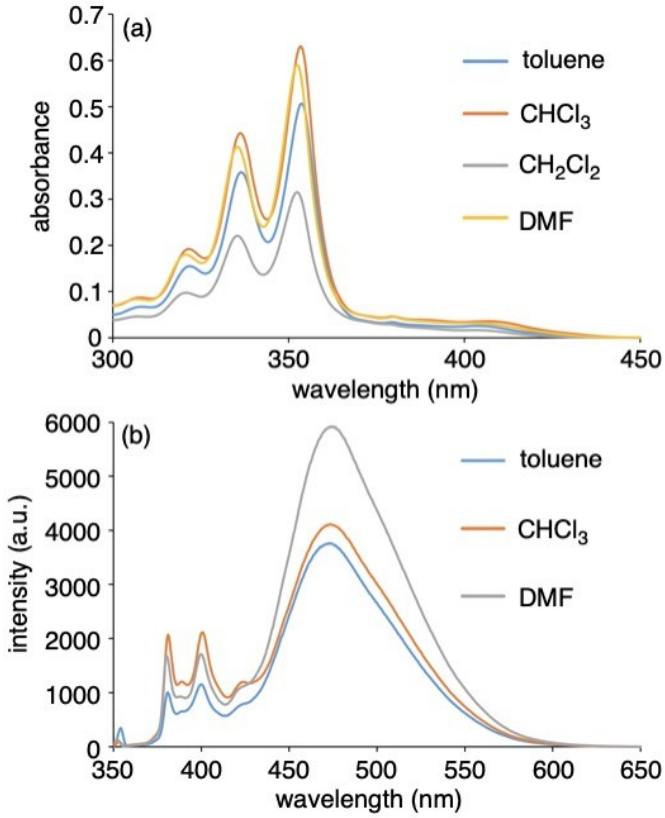

Fig. S3 (a) UV-vis absorption and (b) fluorescence spectra of **4**, 1.0 × 10^{-5} M, λ_{ex} = 352 (in DMF), 353 (in $CHCl_3$), and 354 (in toluene) nm.

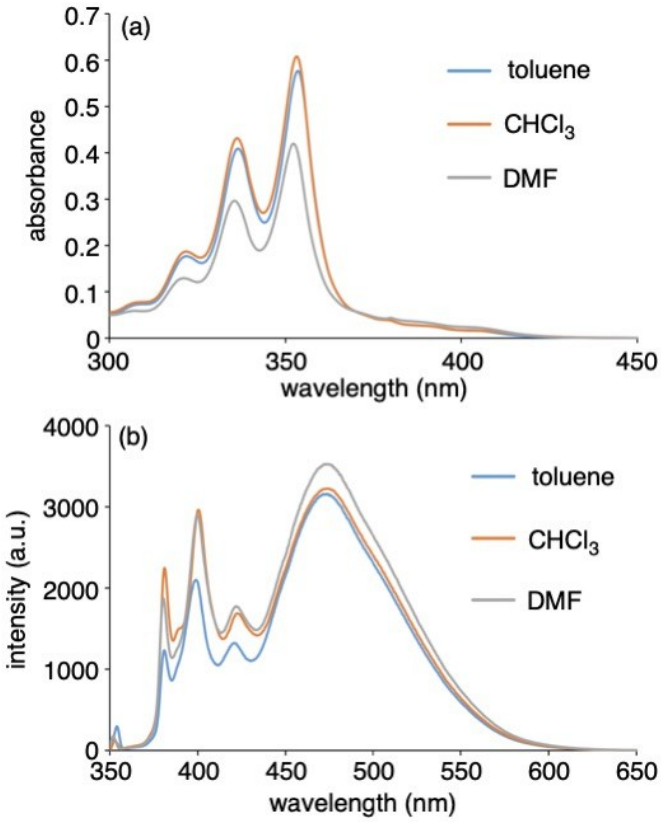

Fig. S4 (a) UV-vis absorption and (b) fluorescence spectra of **6**, 1.0×10^{-5} M, λ_{ex} = 352 (in DMF), 353 (in $CHCl_3$), and 354 (in toluene) nm.

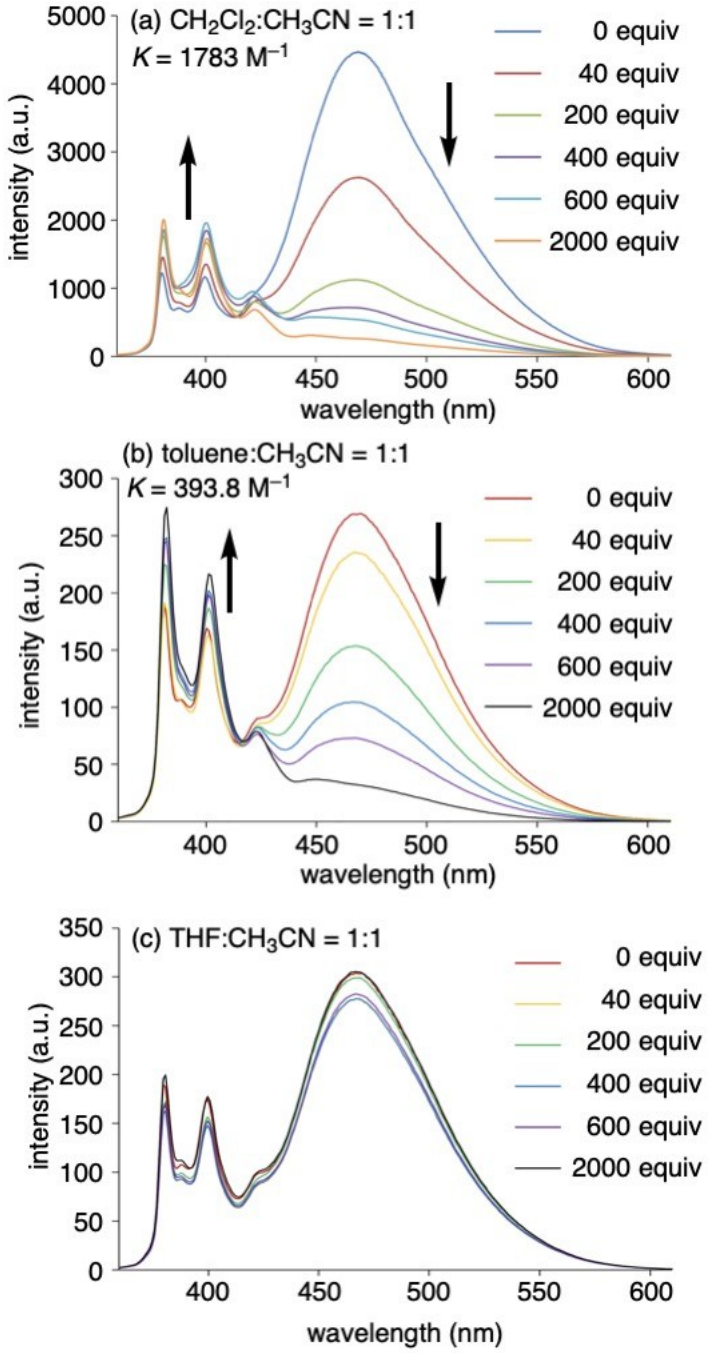

Fig. S5 Fluorescence spectra of **1**, 1.0×10^{-5} M in (a) 1:1 CH_2Cl_2:CH_3CN, (b) 1:1 toluene:CH_3CN, and (c) 1:1 THF:CH_3CN, upon addition of $Ba(ClO_4)_2$ (0-2000 equiv), λ_{ex} = (a)(c) 351, (b) 352 nm.

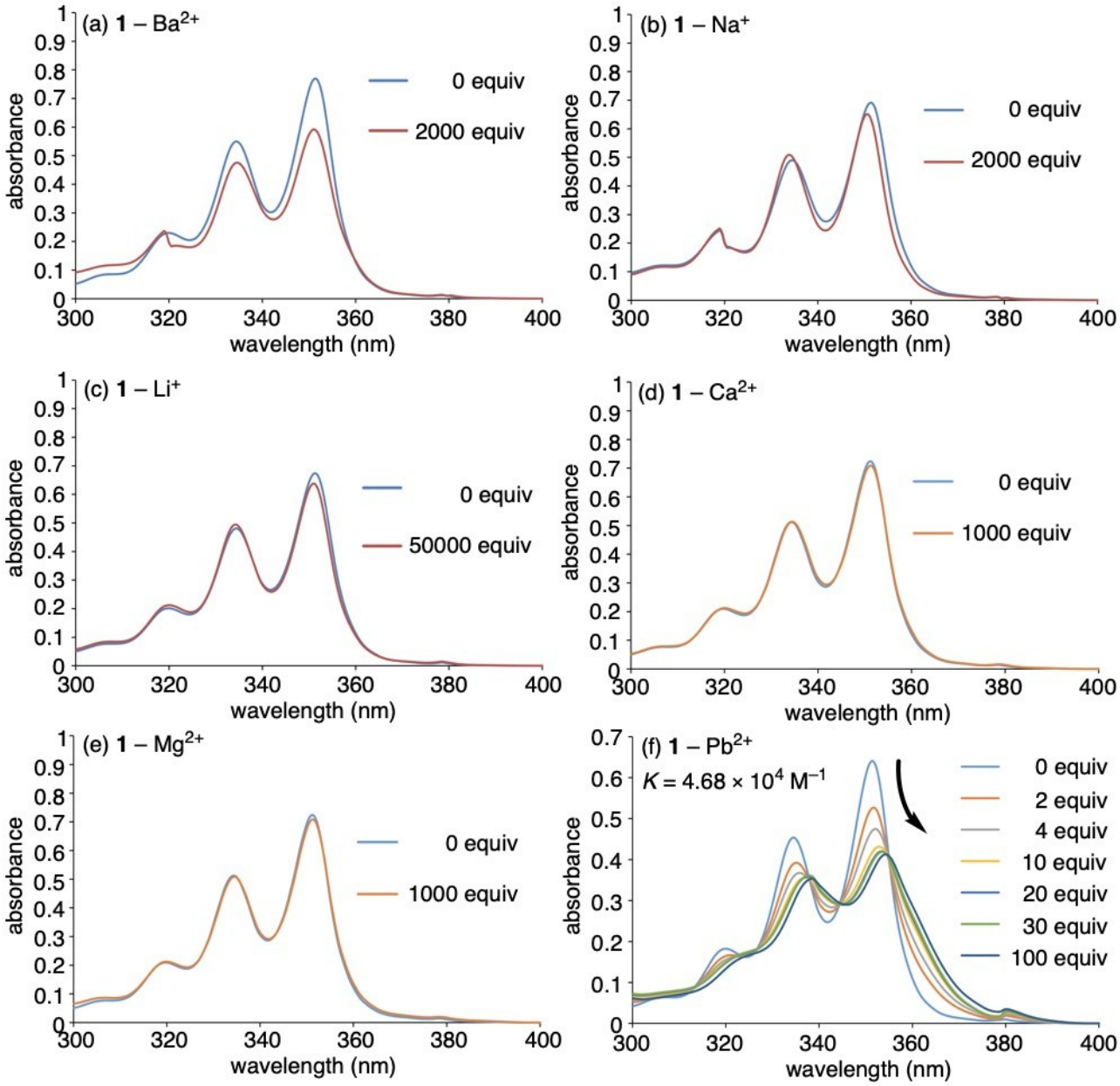

Fig. S6 UV-vis absorption spectra of **1** (1.0×10^{-5} M in 1:1 CH_2Cl_2:CH_3CN) upon addition of (a) $Ba(ClO_4)_2$ (0-2000 equiv), (b) $NaClO_4$ (0-2000 equiv), (c) $LiClO_4$ (0-50000 equiv), (d) $Ca(ClO_4)_2$ (0-1000 equiv), (e) $Mg(ClO_4)_2$ (0-1000 equiv), (f) $Pb(ClO_4)_2$ (0-100 equiv).

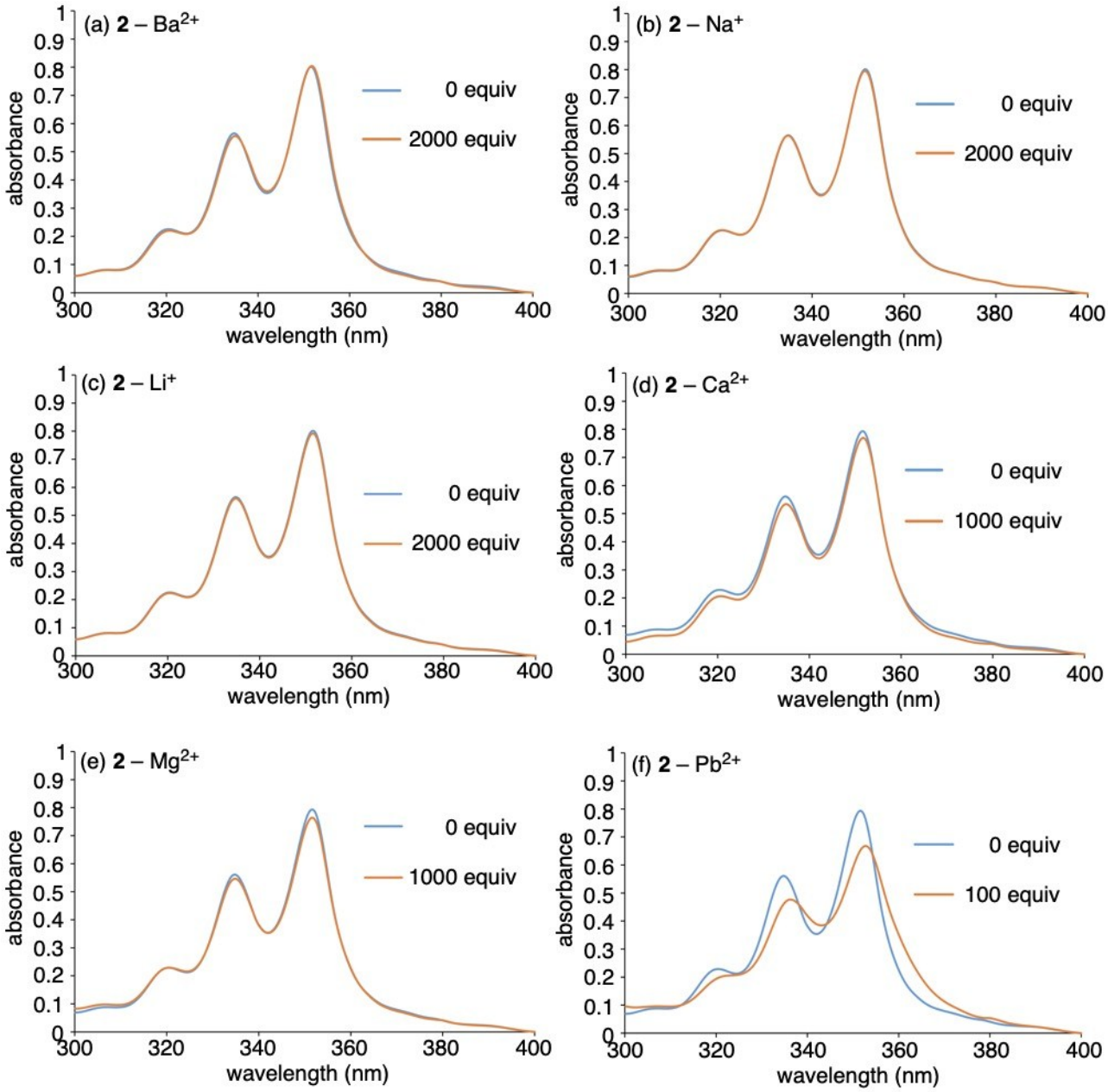

Fig. S7 UV-vis absorption spectra of **2** (1.0×10^{-5} M in 1:1CH_2Cl_2:CH_3CN) upon addition of (a) $Ba(ClO_4)_2$ (0-2000 equiv), (b) $NaClO_4$ (0-2000 equiv), (c) $LiClO_4$ (0-2000 equiv), (d) $Ca(ClO_4)_2$ (0-1000 equiv), (e) $Mg(ClO_4)_2$ (0-1000 equiv), (f) $Pb(ClO_4)_2$ (0-100 equiv).

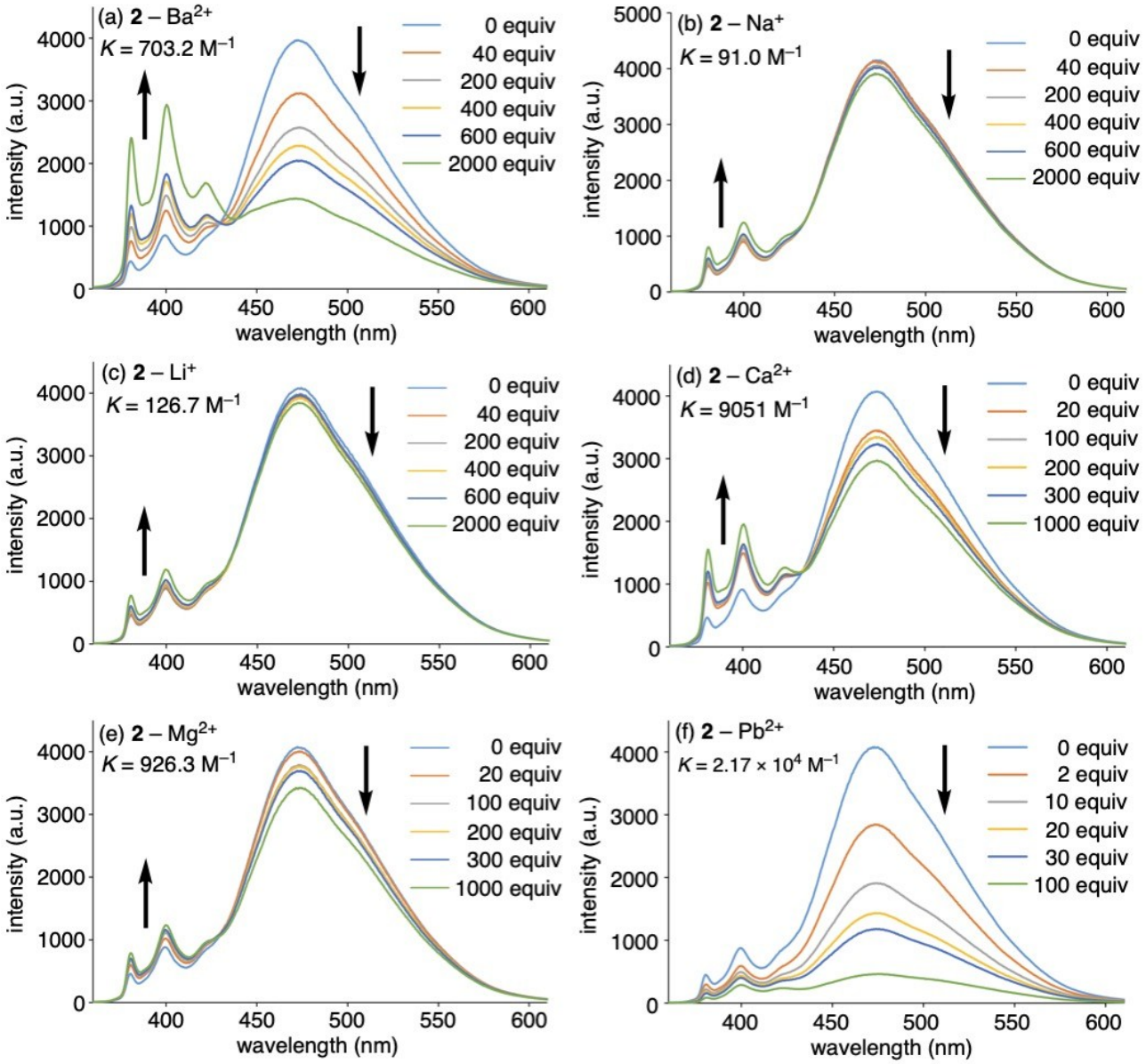

Fig. S8 Fluorescence spectra of **2** (1.0×10^{-5} M in 1:1 CH_2Cl_2:CH_3CN, λ_{ex} = (a)(b)(c)(e)(f) 352 nm, (d) 351 nm) upon addition of (a) $Ba(ClO_4)_2$ (0-2000 equiv), (b) $NaClO_4$ (0-2000 equiv), (c) $LiClO_4$ (0-2000 equiv), (d) $Ca(ClO_4)_2$ (0-1000 equiv), (e) $Mg(ClO_4)_2$ (0-1000 equiv), (f) $Pb(ClO_4)_2$ (0-100 equiv).

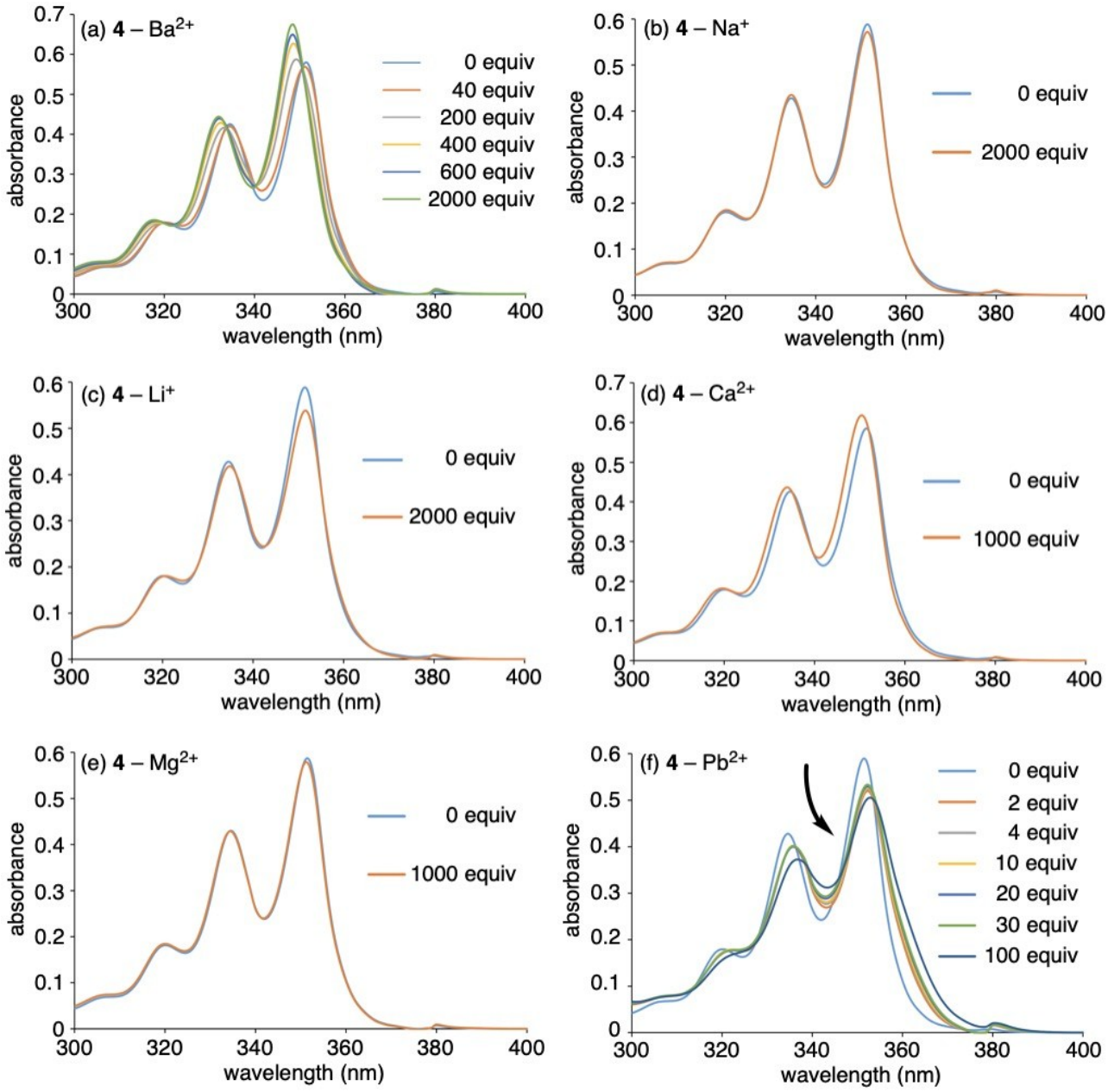

Fig. S9 UV-vis absorption spectra of **4** (1.0×10^{-5} M in 1:1 CH_2Cl_2:CH_3CN) upon addition of (a) $Ba(ClO_4)_2$ (0-2000 equiv), (b) $NaClO_4$ (0-2000 equiv), (c) $LiClO_4$ (0-2000 equiv), (d) $Ca(ClO_4)_2$ (0-1000 equiv), (e) $Mg(ClO_4)_2$ (0-1000 equiv), (f) $Pb(ClO_4)_2$ (0-100 equiv).

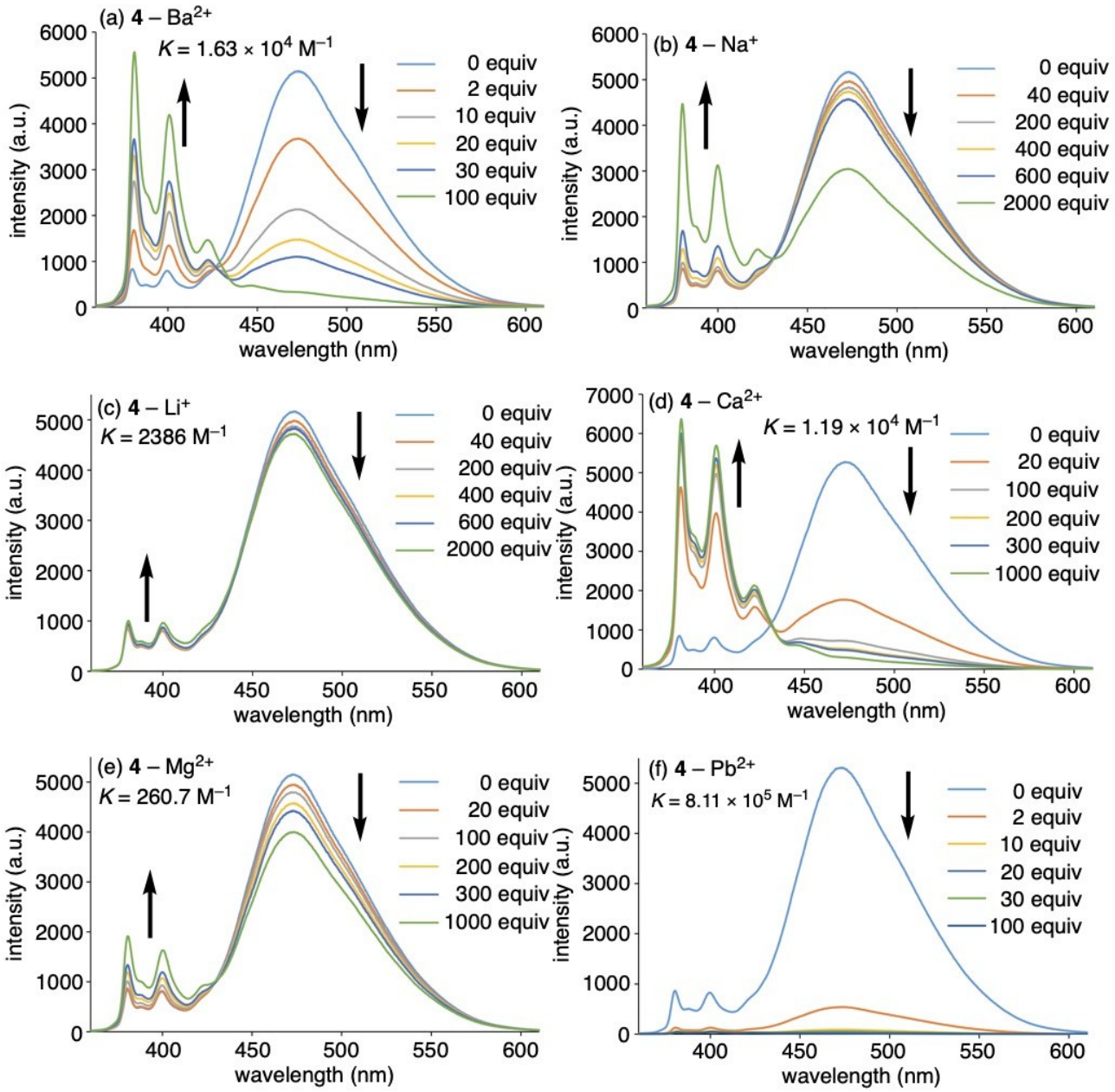

Fig. S10 Fluorescence spectra of **4** (1.0×10^{-5} M in 1:1CH_2Cl_2:CH_3CN, λ_{ex} = 351 nm) upon addition of (a) $Ba(ClO_4)_2$ (0-100 equiv), (b) $NaClO_4$ (0-2000 equiv), (c) $LiClO_4$ (0-2000 equiv), (d) $Ca(ClO_4)_2$ (0-1000 equiv), (e) $Mg(ClO_4)_2$ (0-1000 equiv), (f) $Pb(ClO_4)_2$ (0-100 equiv).

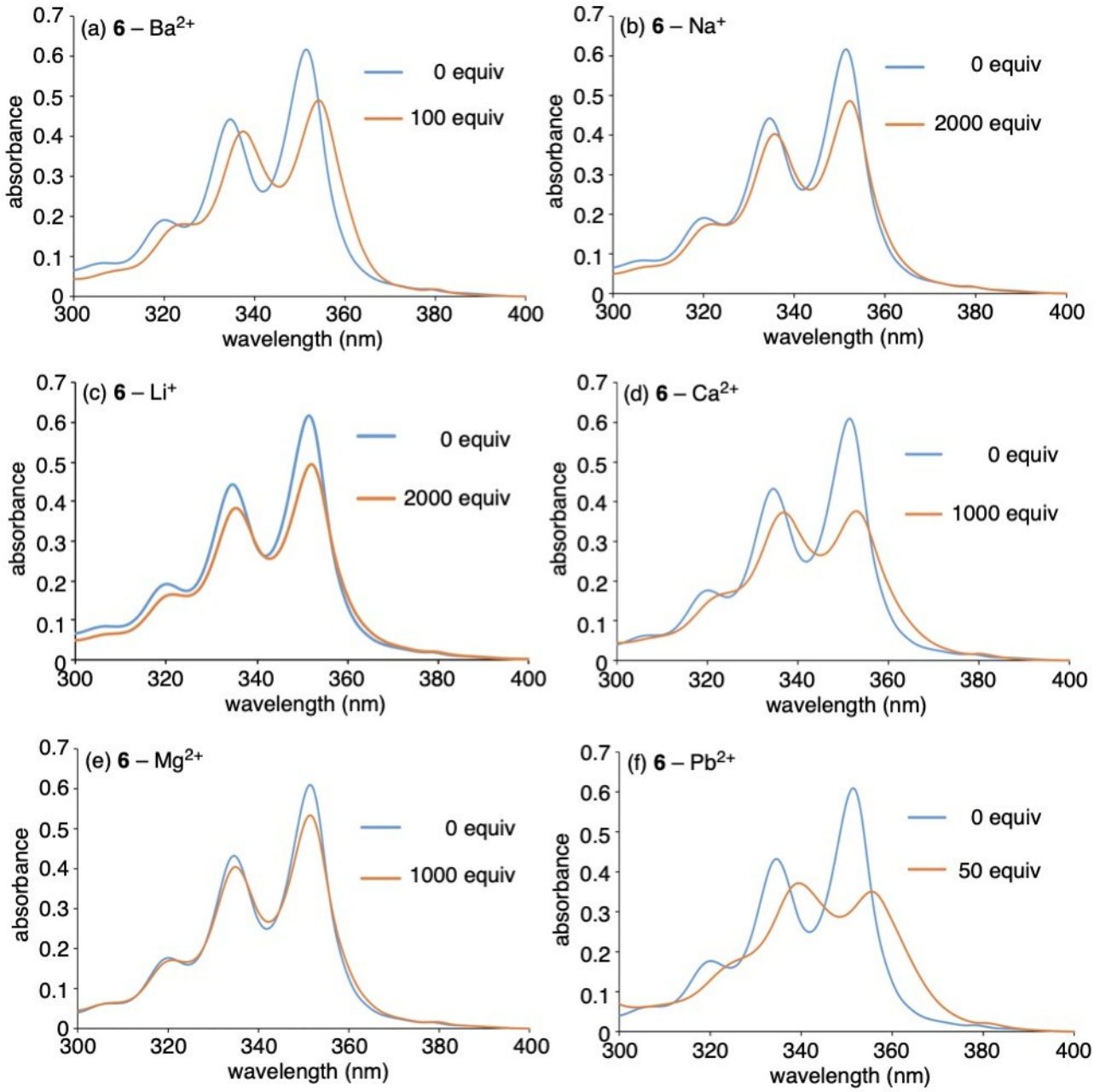

Fig. S11 (a) UV-vis absorption spectra of **6** (1.0×10^{-5} M in 1:1 CH_2Cl_2:CH_3CN) upon addition of (a) $Ba(ClO_4)_2$ (0-100 equiv), (b) $NaClO_4$ (0-2000 equiv), (c) $LiClO_4$ (0-2000 equiv), (d) $Ca(ClO_4)_2$ (0-1000 equiv), (e) $Mg(ClO_4)_2$ (0-1000 equiv), (f) $Pb(ClO_4)_2$ (0-100 equiv).

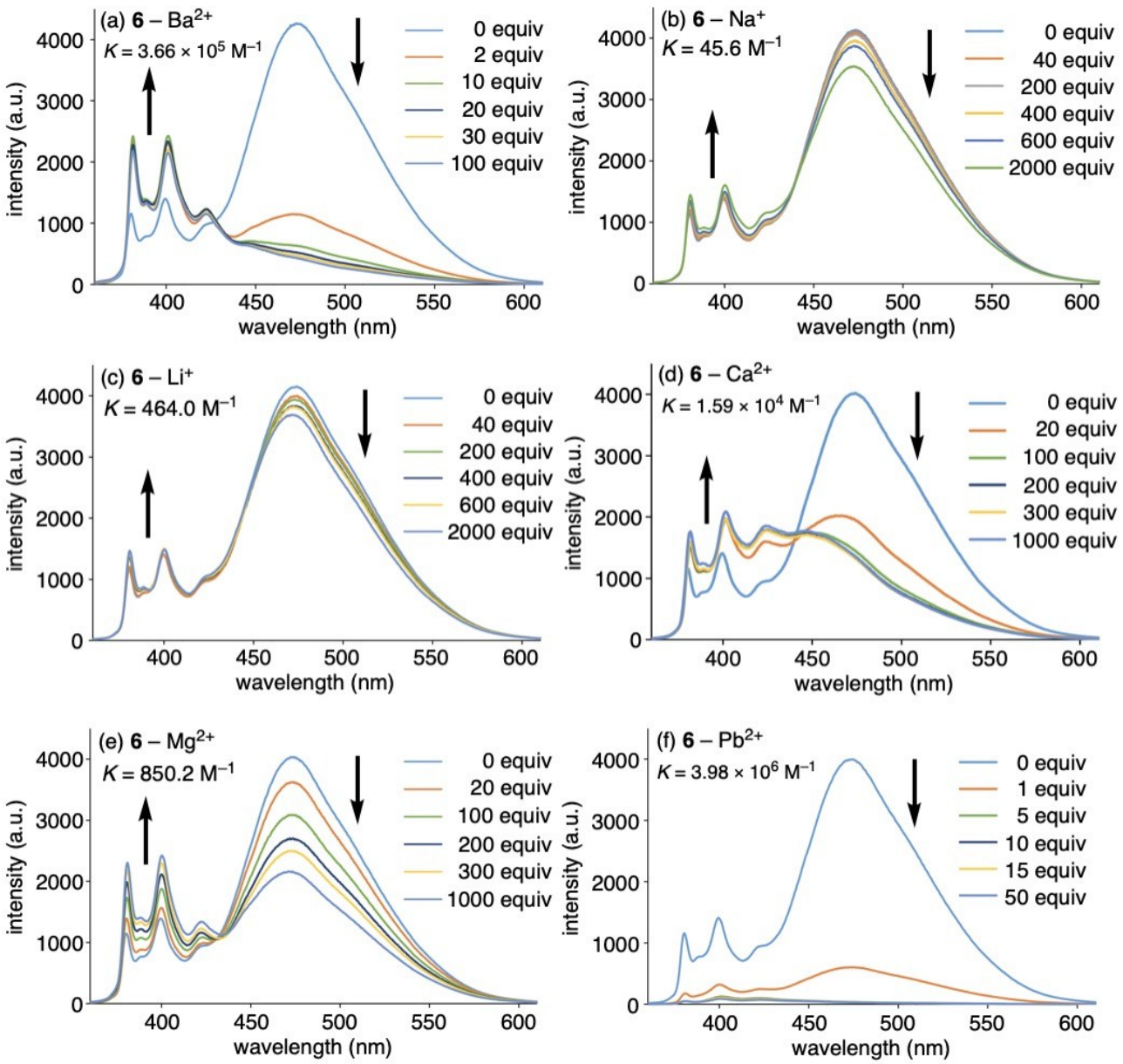

Fig. S12 Fluorescence spectra of **6** (1.0×10^{-5} M in 1:1 CH_2Cl_2:CH_3CN, λ_{ex} = 351 nm) upon addition of (a) $Ba(ClO_4)_2$ (0-100 equiv), (b) $NaClO_4$ (0-2000 equiv), (c) $LiClO_4$ (0-2000 equiv), (d) $Ca(ClO_4)_2$ (0-1000 equiv), (e) $Mg(ClO_4)_2$ (0-1000 equiv), (f) $Pb(ClO_4)_2$ (0-50 equiv).

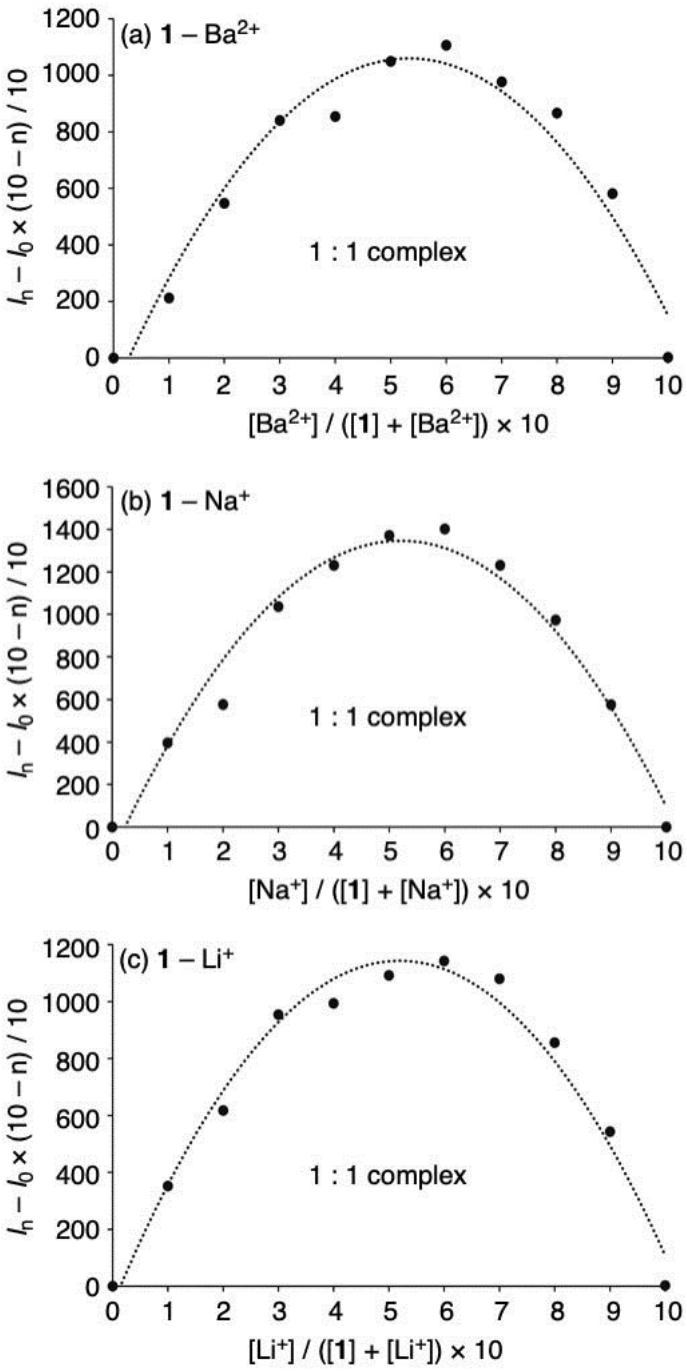

Fig. S13 Job's plots for complex formation between **1** and (a) Ba^{2+}, (b) Na^{+}, (c) Li^{+}, obtained using measurements of fluorescence intensities at 468 nm in 1:1 CH_2Cl_2:CH_3CN, [**1**] + [$M^{n+}(ClO_4^-)_n$] = 1.0×10^{-5} M.

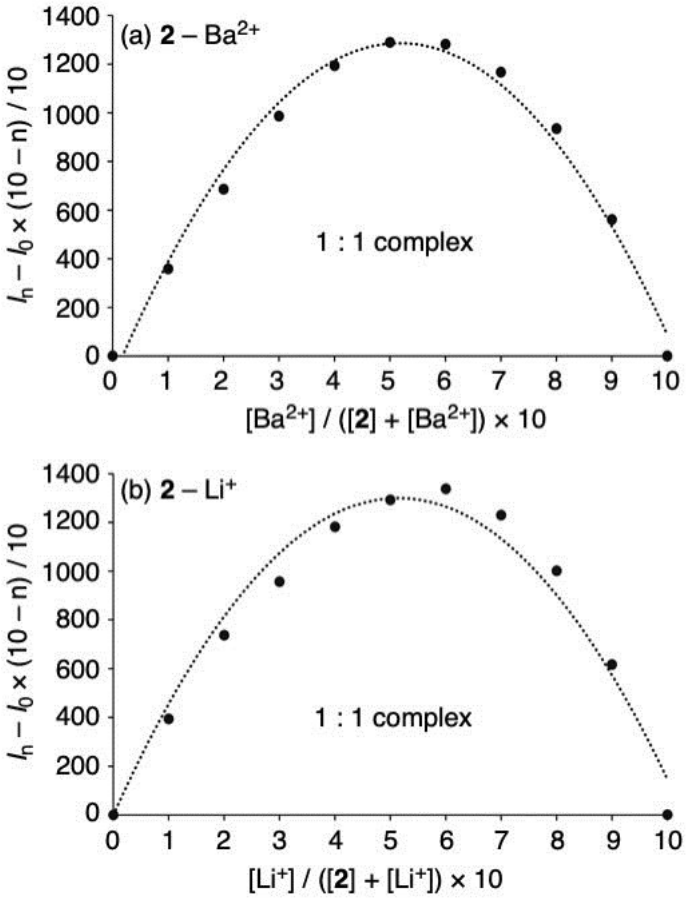

Fig. S14 Job's plots for complex formation between **2** and (a) Ba^{2+}, (b) Li^{+}, obtained using measurements of fluorescence intensities at 473 nm in 1:1 CH_2Cl_2:CH_3CN, [**2**] + [$M^{n+}(ClO_4^-)_n$] = 1.0×10^{-5} M.

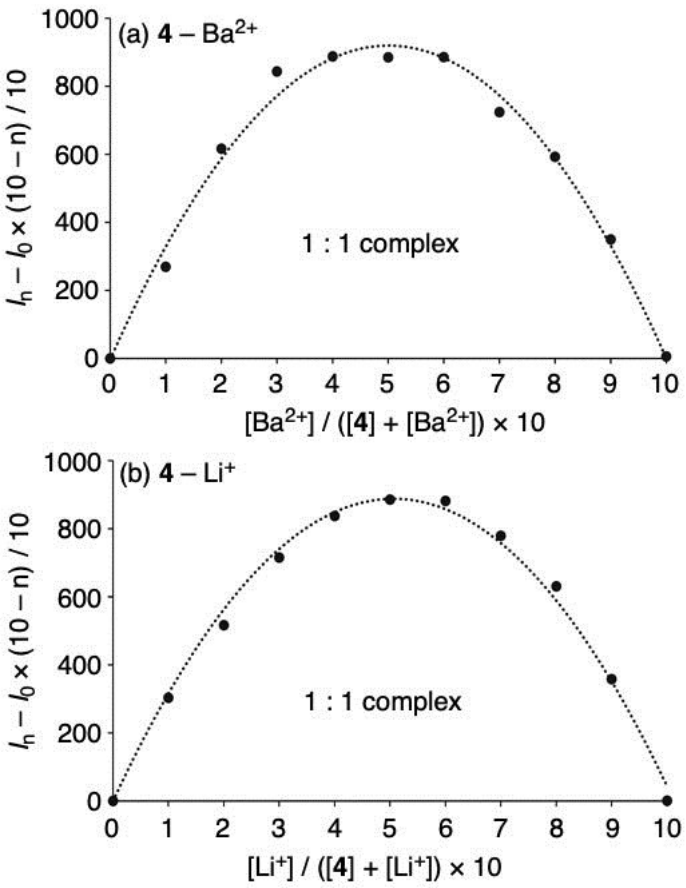

Fig. S15 Job's plots for complex formation between **4** and (a) Ba^{2+}, (b) Li^{+}, obtained using measurements of fluorescence intensities at 472 nm in 1:1 CH_2Cl_2:CH_3CN, [**4**] + [$M^{n+}(ClO_4^{-})_n$] = 1.0×10^{-5} M.

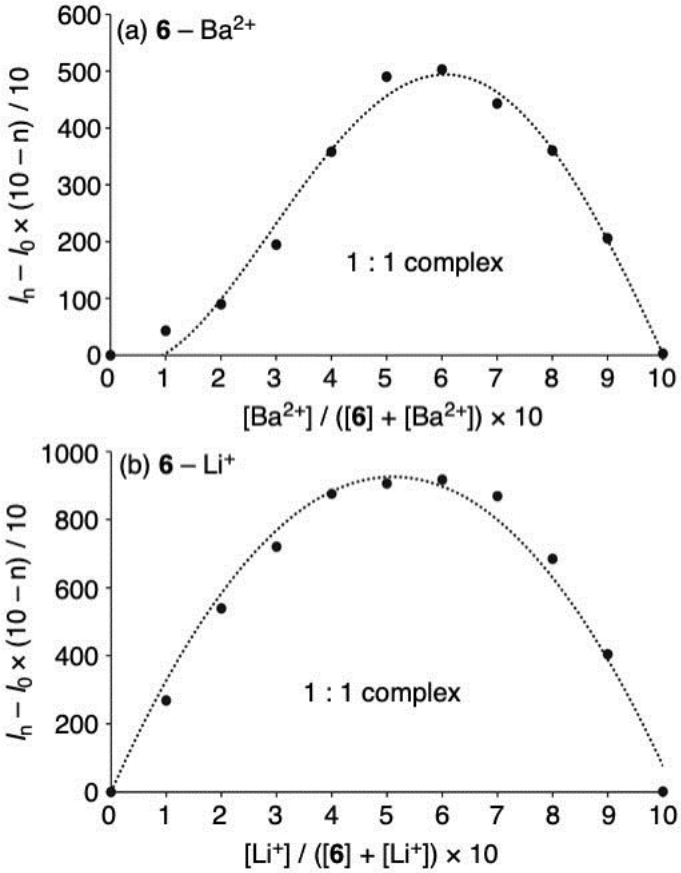

Fig. S16 Job's plots for complex formation between **6** and (a) Ba^{2+}, (b) Li^{+}, obtained using measurements of fluorescence intensities at (a) 380, (b) 472 nm in 1:1 CH_2Cl_2:CH_3CN, [**6**] + [$M^{n+}(ClO_4^-)_n$] = 1.0×10^{-5} M.

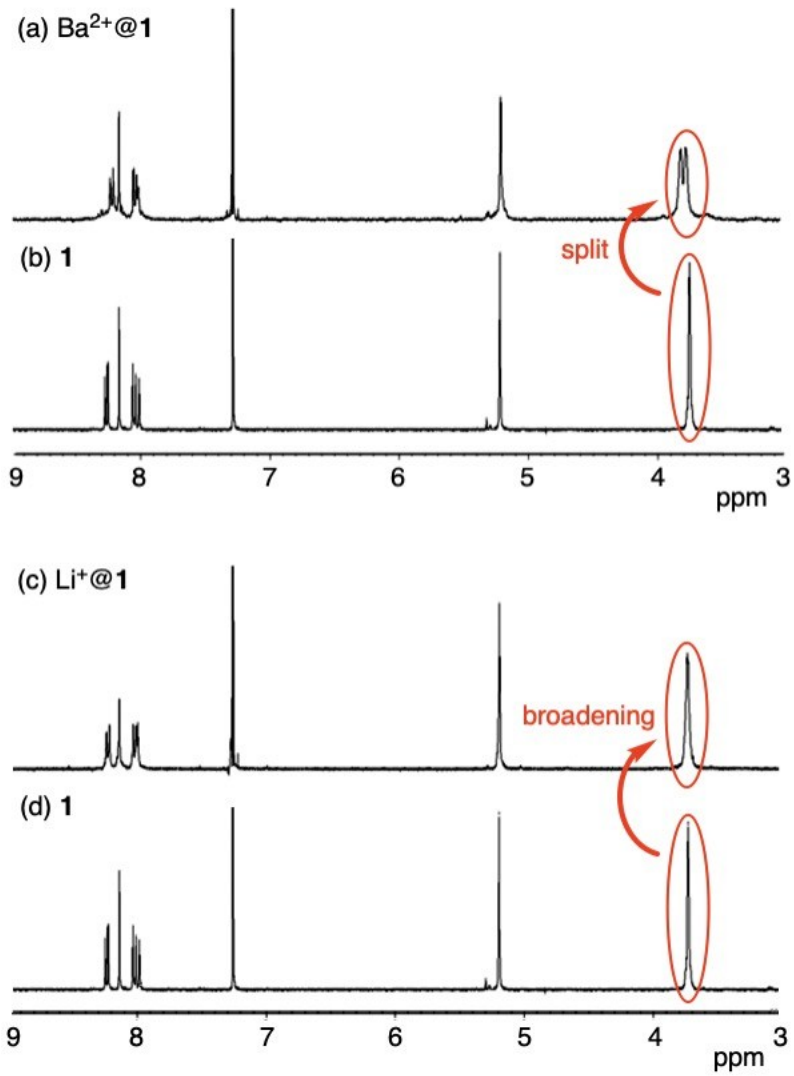

Fig. S17 ^{1}H NMR spectra (400 MHz, $CDCl_3$) of (a) a mixture of **1** with $Ba(ClO_4)_2$, (b) **1**, (c) a mixture of **1** with $LiClO_4$, and (d) **1**.

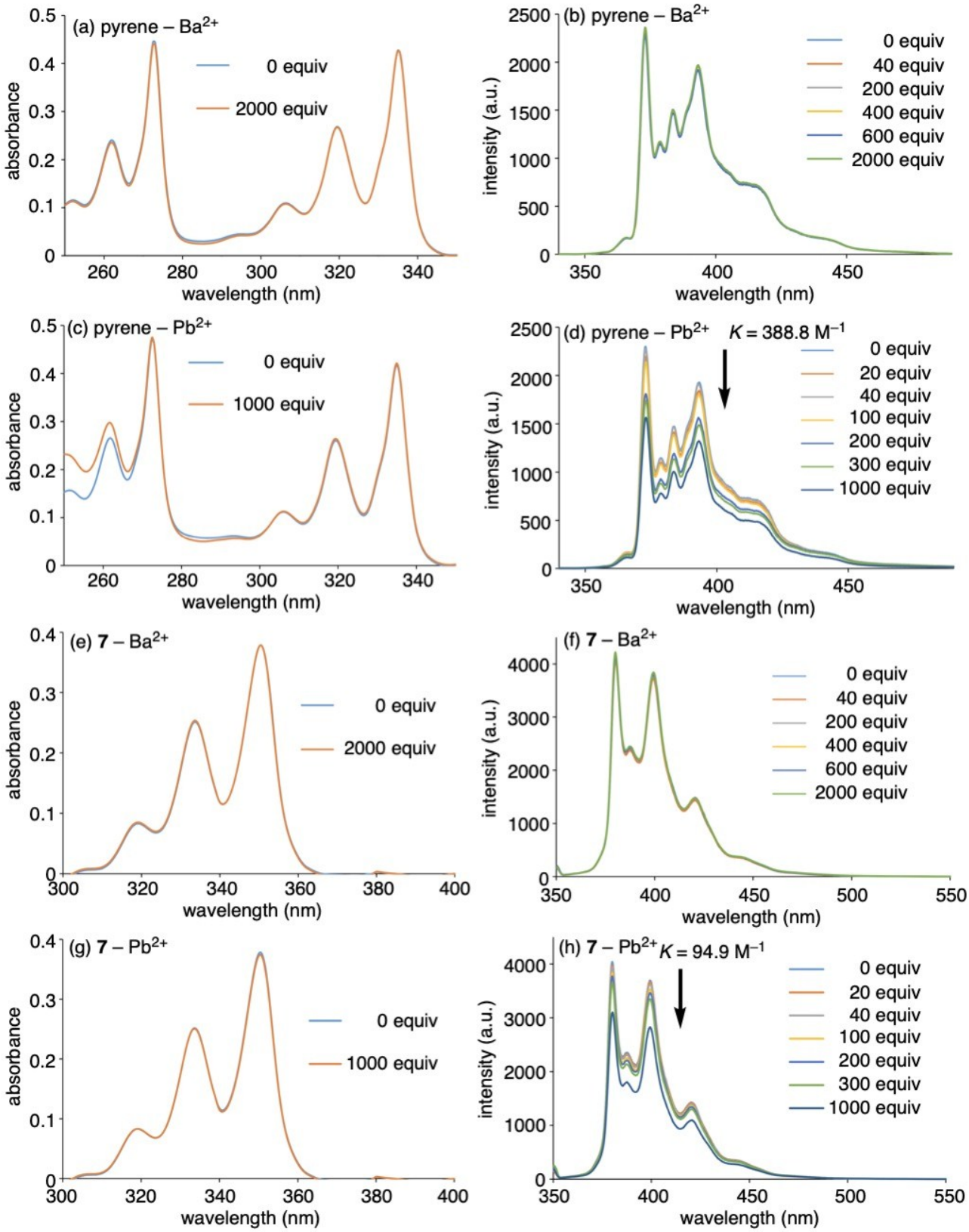

Fig. S18 (a)(c) UV-vis absorption spectra of pyrene (**8**, 1.0 × 10^{-5} M in 1:1 CH_2Cl_2:CH_3CN) upon addition of (a) $Ba(ClO_4)_2$ (0-2000 equiv) and (c) $Pb(ClO_4)_2$ (0-1000 equiv). (b)(d) Fluorescence spectra of pyrene (**8**, 1.0 × 10^{-5} M in 1:1 CH_2Cl_2:CH_3CN, λ_{ex} = 335 nm) upon addition of (b) $Ba(ClO_4)_2$ (0-2000 equiv) and (d) $Pb(ClO_4)_2$ (0-1000 equiv). (e)(g) UV-vis absorption spectra of **7** (1.0 × 10^{-5} M in 1:1 CH_2Cl_2:CH_3CN) upon addition of (e) $Ba(ClO_4)_2$ (0-2000 equiv) and (g) $Pb(ClO_4)_2$ (0-1000 equiv). (f)(h) Fluorescence spectra of **7** (1.0 × 10^{-5} M in 1:1 CH_2Cl_2:CH_3CN, λ_{ex} = 350 nm) upon addition of (f) $Ba(ClO_4)_2$ (0-2000 equiv) and (h) $Pb(ClO_4)_2$ (0-1000 equiv).

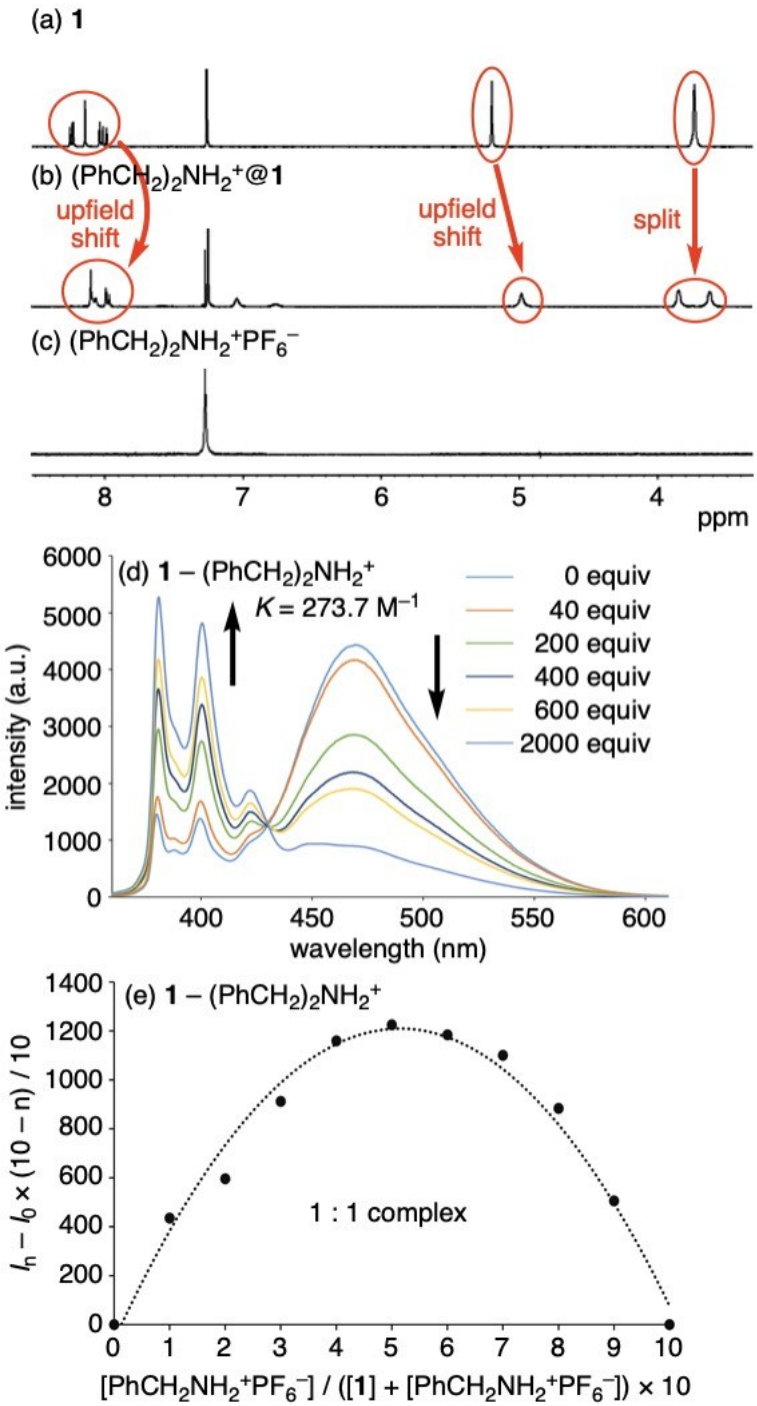

Fig. S19 ^{1}H NMR spectra (400 MHz, $CDCl_3$) of (a) **1**, (b) a mixture of **1** with $(PhCH_2)_2NH_2^+PF_6^-$, and (c) $(PhCH_2)_2NH_2^+PF_6^-$. (d) Fluorescence spectra of **1** (1.0×10^{-5} M in 1:1 CH_2Cl_2:CH_3CN, λ_{ex} = 351 nm) upon addition of $(PhCH_2)_2NH_2^+PF_6^-$ (0-2000 equiv). (e) Job's plot for complex formation between **1** and $(PhCH_2)_2NH_2^+PF_6^-$, obtained using measurements of fluorescence intensities at 468 nm in 1:1 CH_2Cl_2:CH_3CN, [**1**] + [$(PhCH_2)_2NH_2^+PF_6^-$] = 1.0×10^{-5} M.

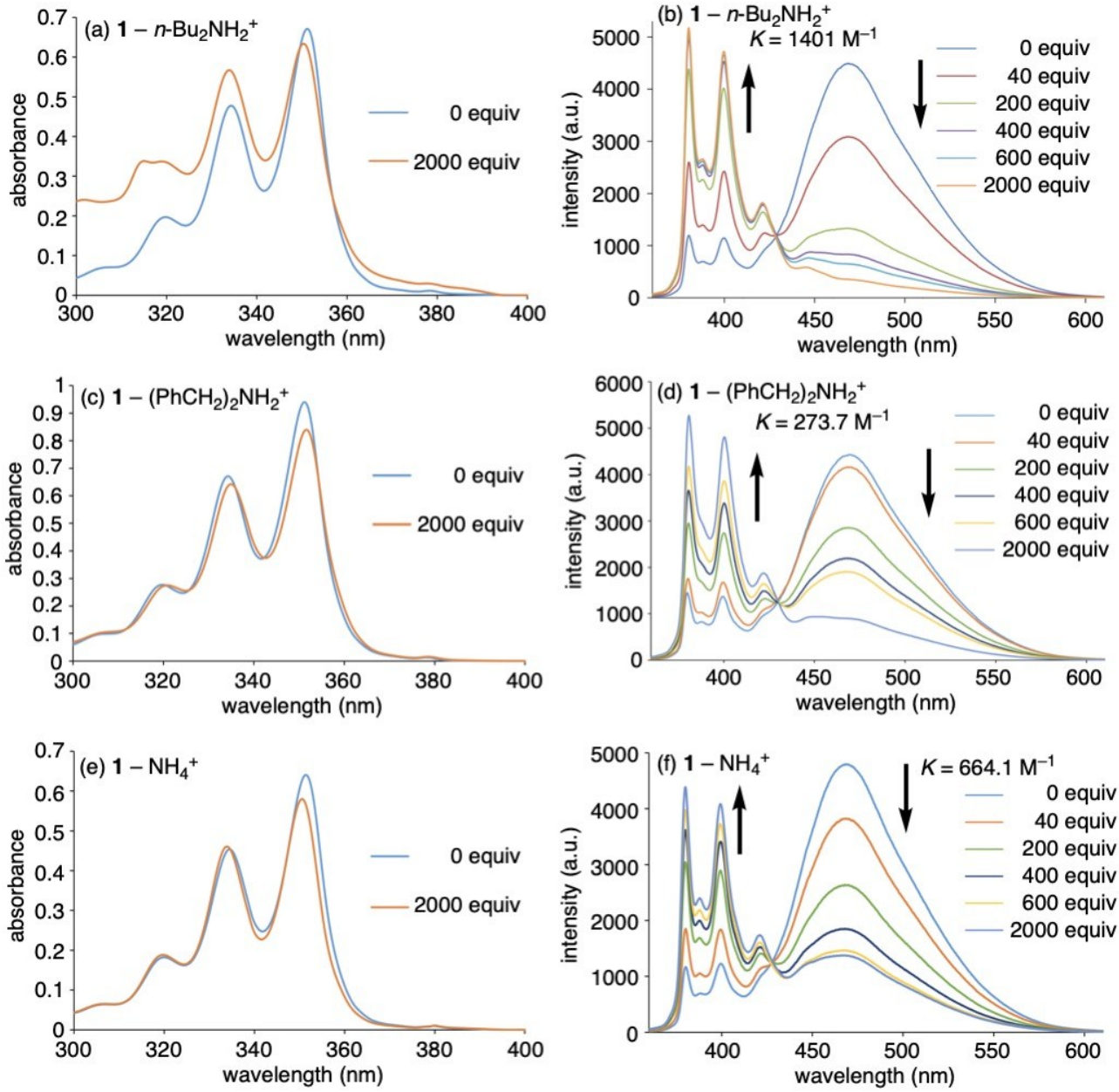

Fig. S20 (a)(c)(e) UV-vis absorption spectra of **1** (1.0×10^{-5} M in 1:1 CH_2Cl_2:CH_3CN) upon addition of (a) *n*-$Bu_2NH_2^+PF_6^-$ (0-2000 equiv), (c) $(PhCH_2)_2NH_2^+PF_6^-$ (0-2000 equiv), and (e) $NH_4^+PF_6^-$ (0-2000 equiv). (b)(d)(f) Fluorescence spectra of **1** (1.0×10^{-5} M in 1:1 CH_2Cl_2:CH_3CN, λ_{ex} = 351 nm) upon addition of (b) *n*-$Bu_2NH_2^+PF_6^-$ (0-2000 equiv), (d) $(PhCH_2)_2NH_2^+PF_6^-$ (0-2000 equiv), and (f) $NH_4^+PF_6^-$ (0-2000 equiv).

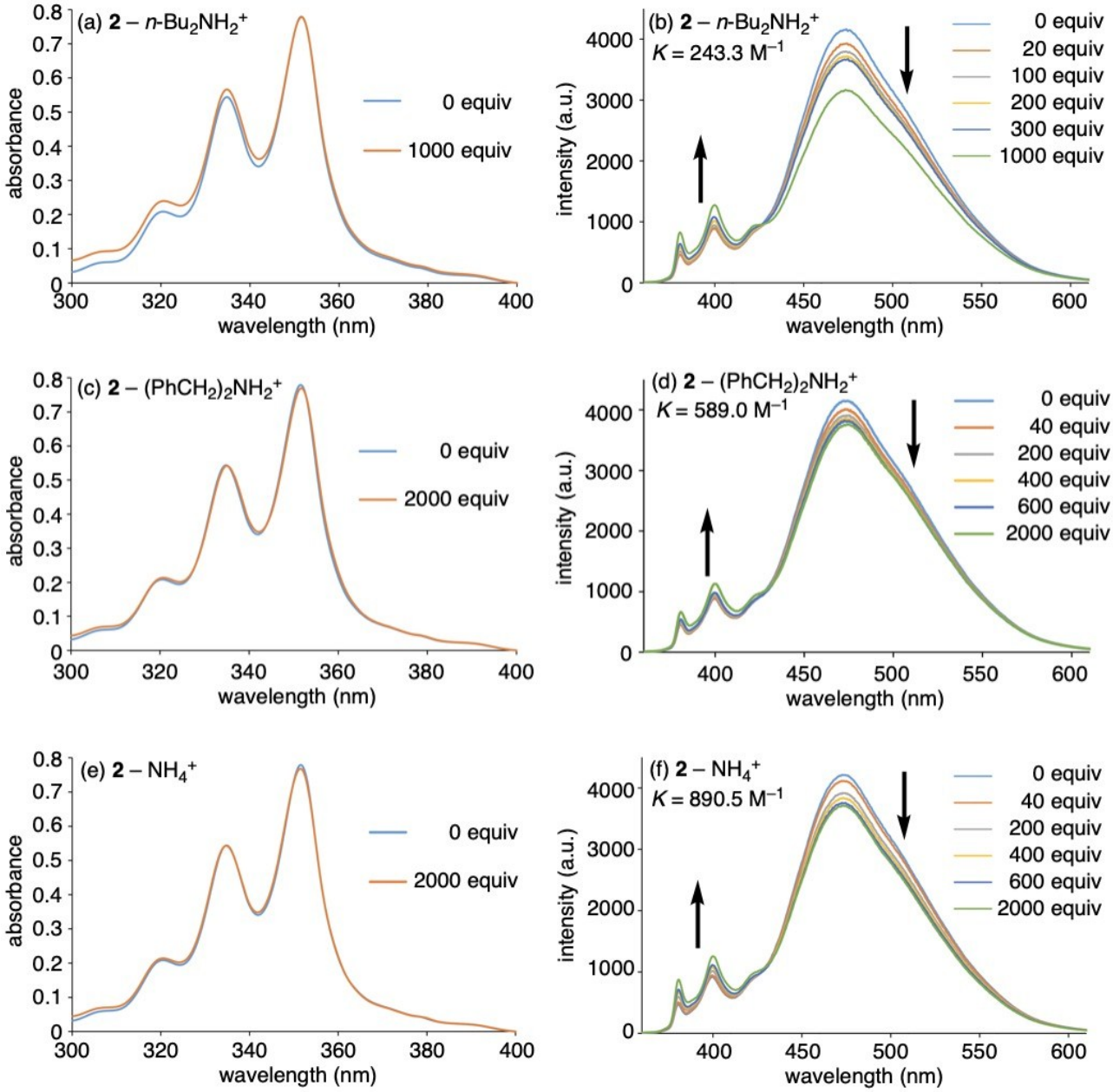

Fig. S21 (a)(c)(e) UV-vis absorption spectra of **2** (1.0×10^{-5} M in 1:1 CH_2Cl_2:CH_3CN) upon addition of (a) *n*-$Bu_2NH_2^+PF_6^-$ (0-1000 equiv), (c) $(PhCH_2)_2NH_2^+PF_6^-$ (0-2000 equiv), and (e) $NH_4^+PF_6^-$ (0-2000 equiv). (b)(d)(f) Fluorescence spectra of **2** (1.0×10^{-5} M in 1:1 CH_2Cl_2:CH_3CN, λ_{ex} = 352 nm) upon addition of (b) *n*-$Bu_2NH_2^+PF_6^-$ (0-1000 equiv), (d) $(PhCH_2)_2NH_2^+PF_6^-$ (0-2000 equiv), and (f) $NH_4^+PF_6^-$ (0-2000 equiv).

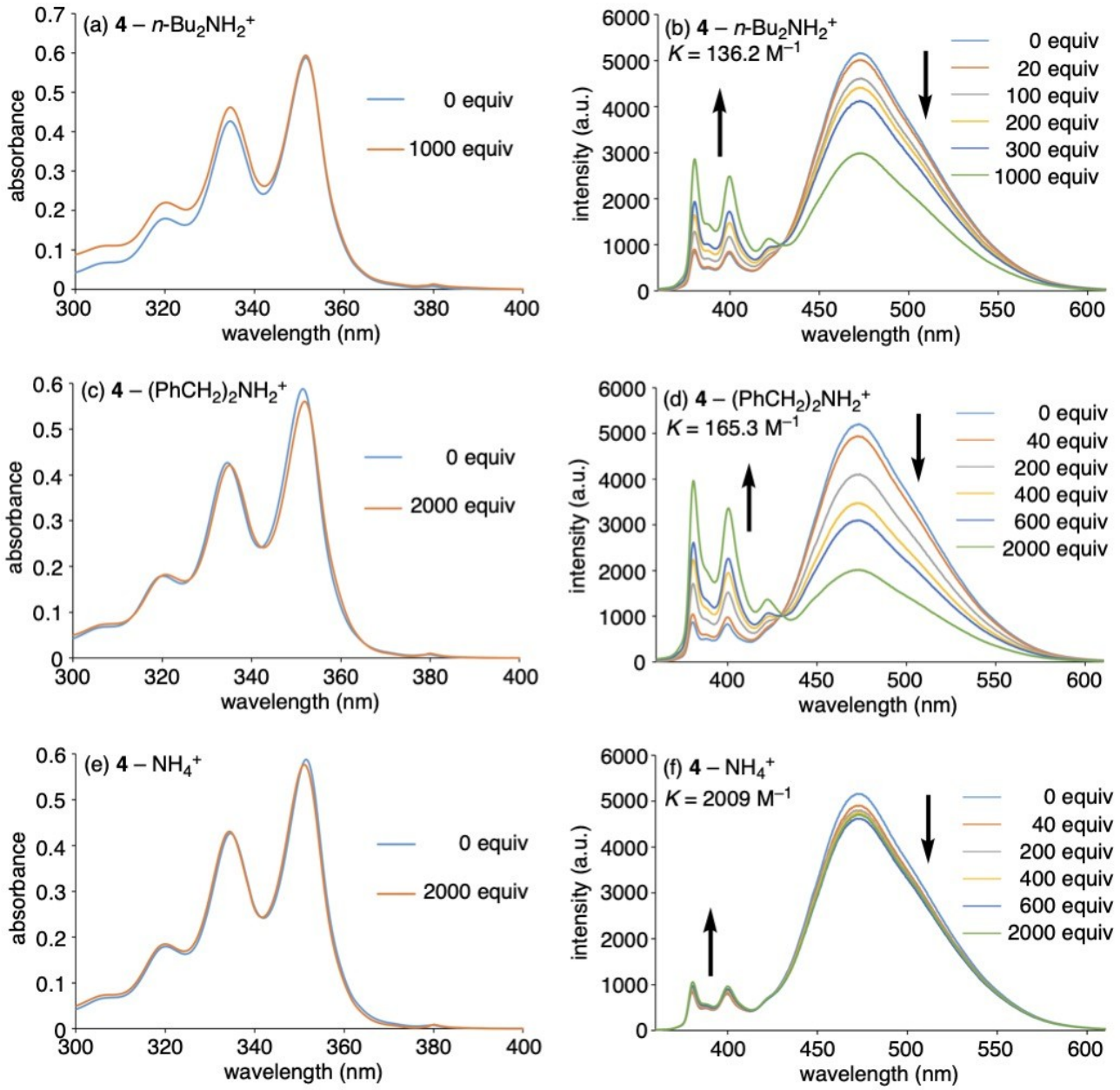

Fig. S22 (a)(c)(e) UV-vis absorption spectra of **4** (1.0×10^{-5} M in 1:1 CH_2Cl_2:CH_3CN) upon addition of (a) *n*-$Bu_2NH_2^+PF_6^-$ (0-1000 equiv), (c) $(PhCH_2)_2NH_2^+PF_6^-$ (0-2000 equiv), and (e) $NH_4^+PF_6^-$ (0-2000 equiv). (b)(d)(f) Fluorescence spectra of **4** (1.0×10^{-5} M in 1:1 CH_2Cl_2:CH_3CN, λ_{ex} = 351 nm) upon addition of (b) *n*-$Bu_2NH_2^+PF_6^-$ (0-1000 equiv), (d) $(PhCH_2)_2NH_2^+PF_6^-$ (0-2000 equiv), and (f) $NH_4^+PF_6^-$ (0-2000 equiv).

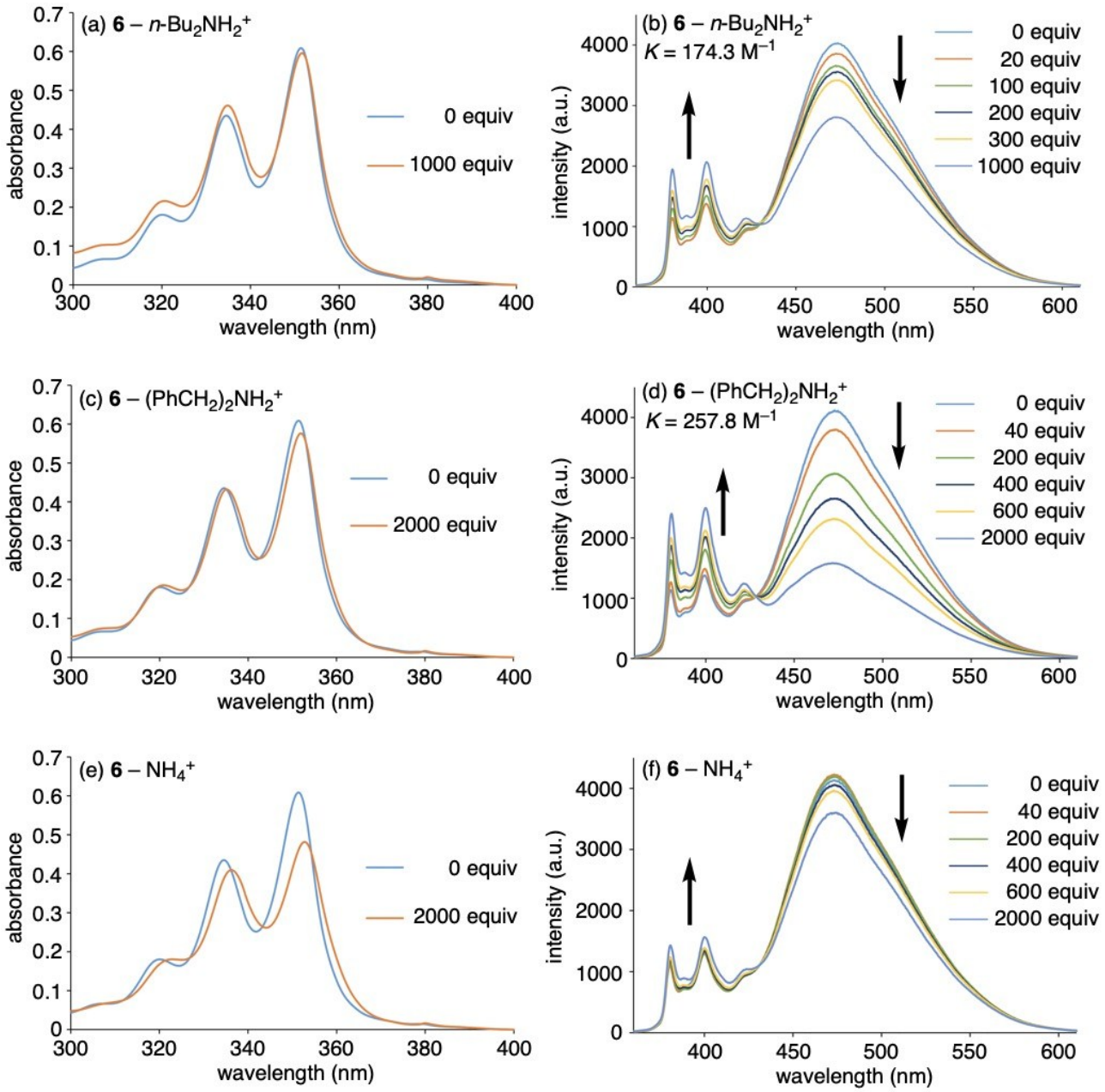

Fig. S23 (a)(c)(e) UV-vis absorption spectra of **6** (1.0×10^{-5} M in 1:1 CH_2Cl_2:CH_3CN) upon addition of (a) *n*-$Bu_2NH_2^+PF_6^-$ (0-1000 equiv), (c) $(PhCH_2)_2NH_2^+PF_6^-$ (0-2000 equiv), and (e) $NH_4^+PF_6^-$ (0-2000 equiv). (b)(d)(f) Fluorescence spectra of **6** (1.0×10^{-5} M in 1:1 CH_2Cl_2:CH_3CN, λ_{ex} = 351 nm) upon addition of (b) *n*-$Bu_2NH_2^+PF_6^-$ (0-1000 equiv), (d) $(PhCH_2)_2NH_2^+PF_6^-$ (0-2000 equiv), and (f) $NH_4^+PF_6^-$ (0-2000 equiv).

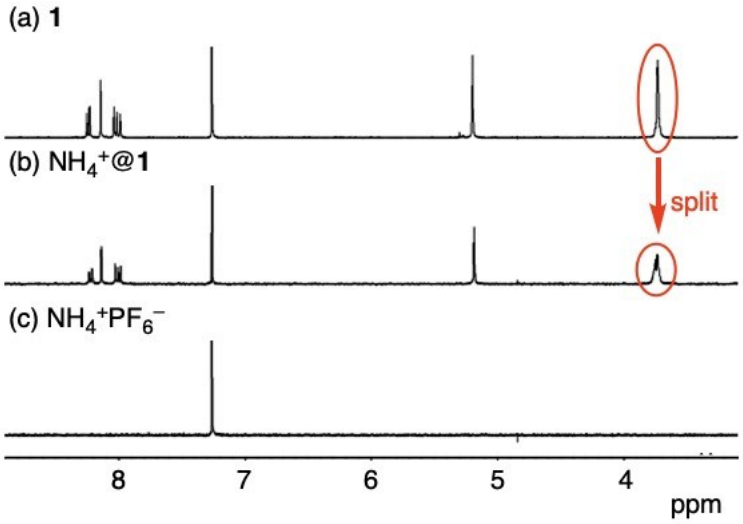

Fig. S24 ^{1}H NMR spectra (400 MHz, $CDCl_3$) of (a) **1**, (b) a mixture of **1** with $NH_4^+PF_6^-$, and (c) $NH_4^+PF_6^-$.

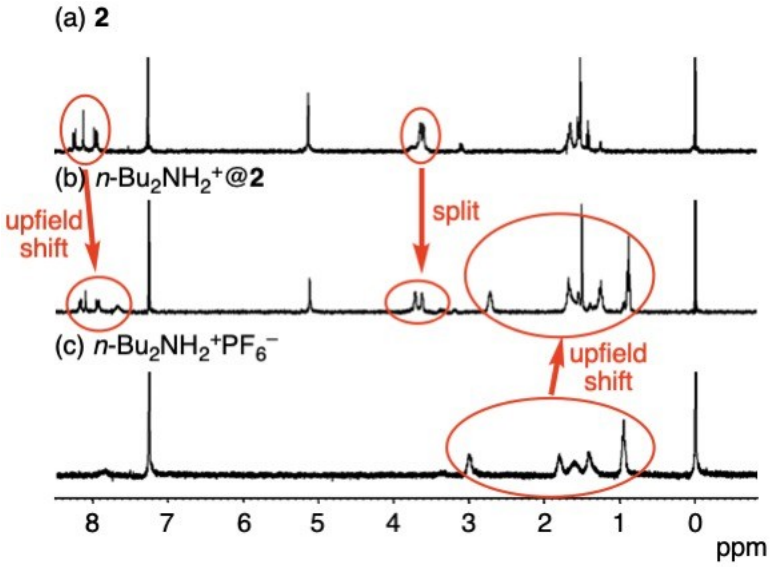

Fig. S25 ^{1}H NMR spectra (400 MHz, $CDCl_3$) of (a) **2**, (b) a mixture of **2** with n-$Bu_2NH_2^+PF_6^-$, and (c) n-$Bu_2NH_2^+PF_6^-$.

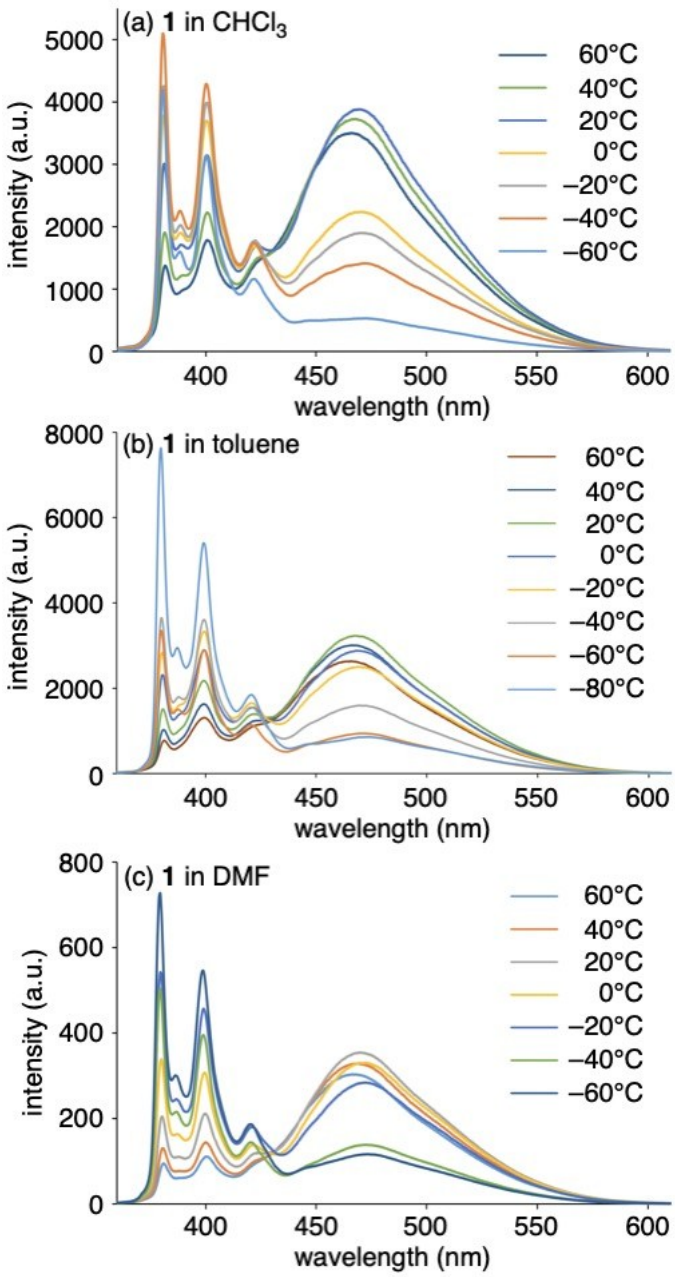

Fig. S26 Variable-temperature fluorescence spectra of **1**, 1.0×10^{-5} M in (a) $CHCl_3$, λ_{ex} = 354 nm, (b) toluene, λ_{ex} = 354 nm, and (c) DMF, λ_{ex} = 352 nm.

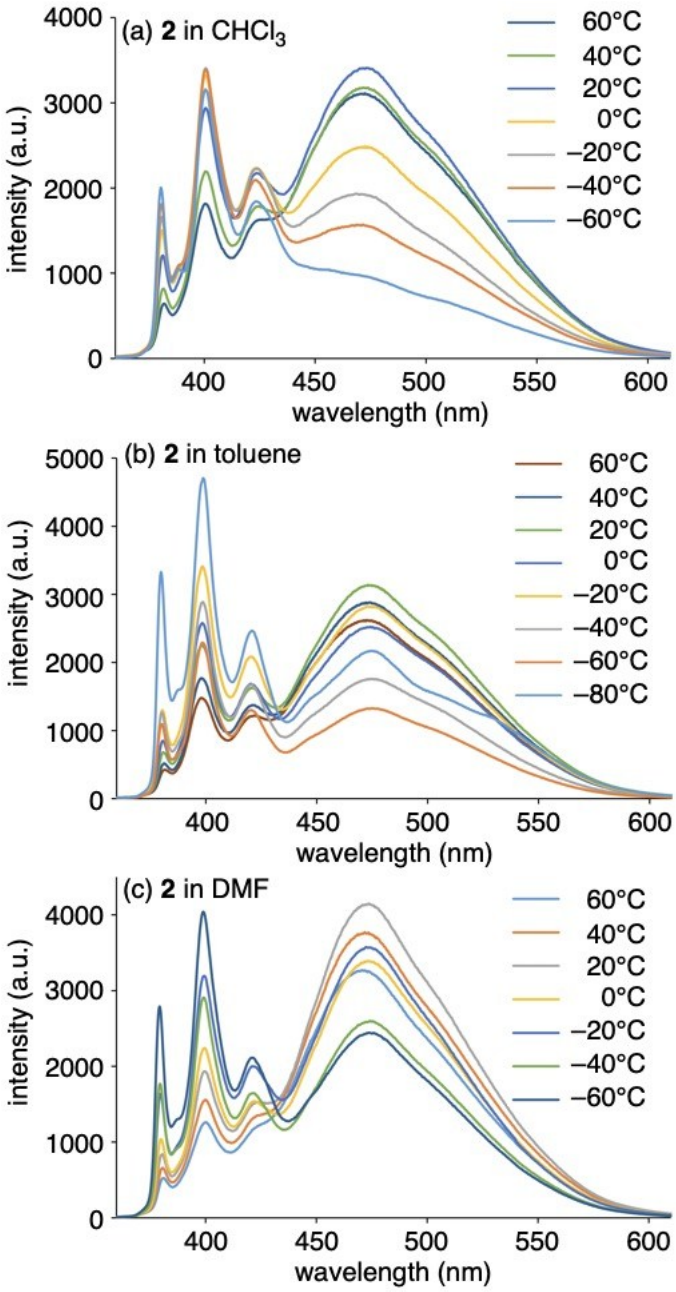

Fig. S27 Variable-temperature fluorescence spectra of **2**, 1.0×10^{-5} M in (a) $CHCl_3$, λ_{ex} = 354 nm, (b) toluene, λ_{ex} = 354 nm, and (c) DMF, λ_{ex} = 353 nm.

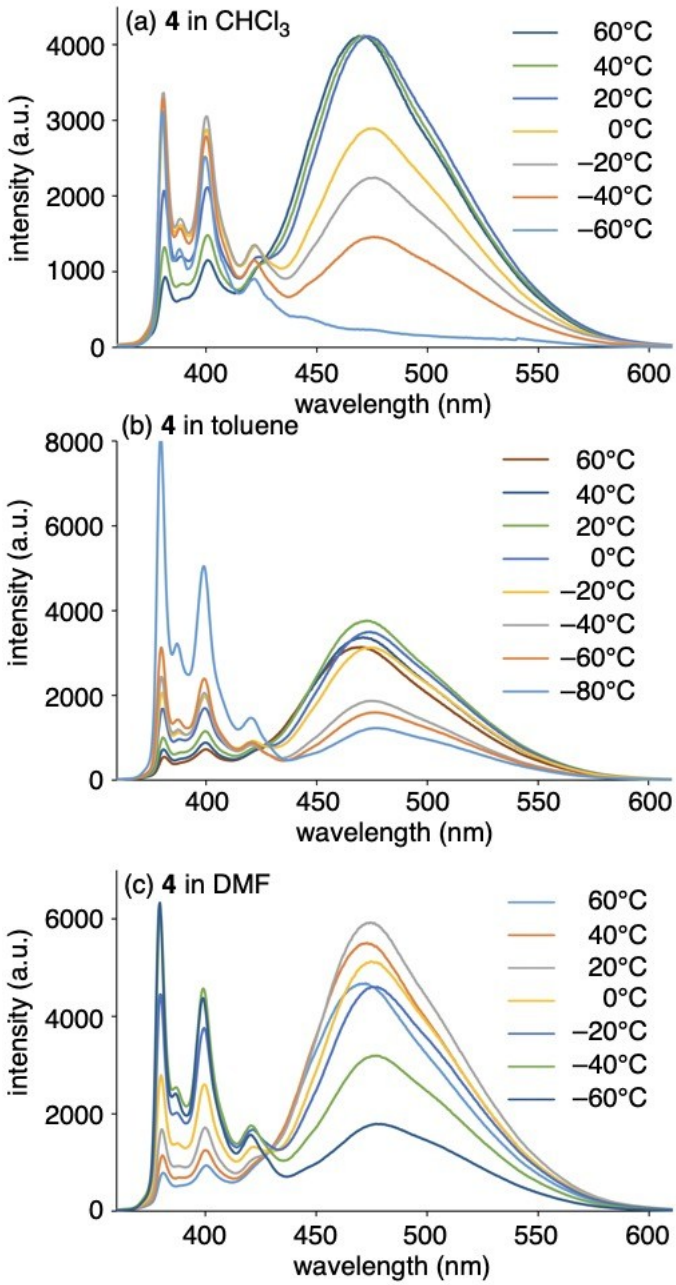

Fig. S28 Variable-temperature fluorescence spectra of **4**, 1.0×10^{-5} M in (a) $CHCl_3$, λ_{ex} = 353 nm, (b) toluene, λ_{ex} = 354 nm, and (c) DMF, λ_{ex} = 352 nm.

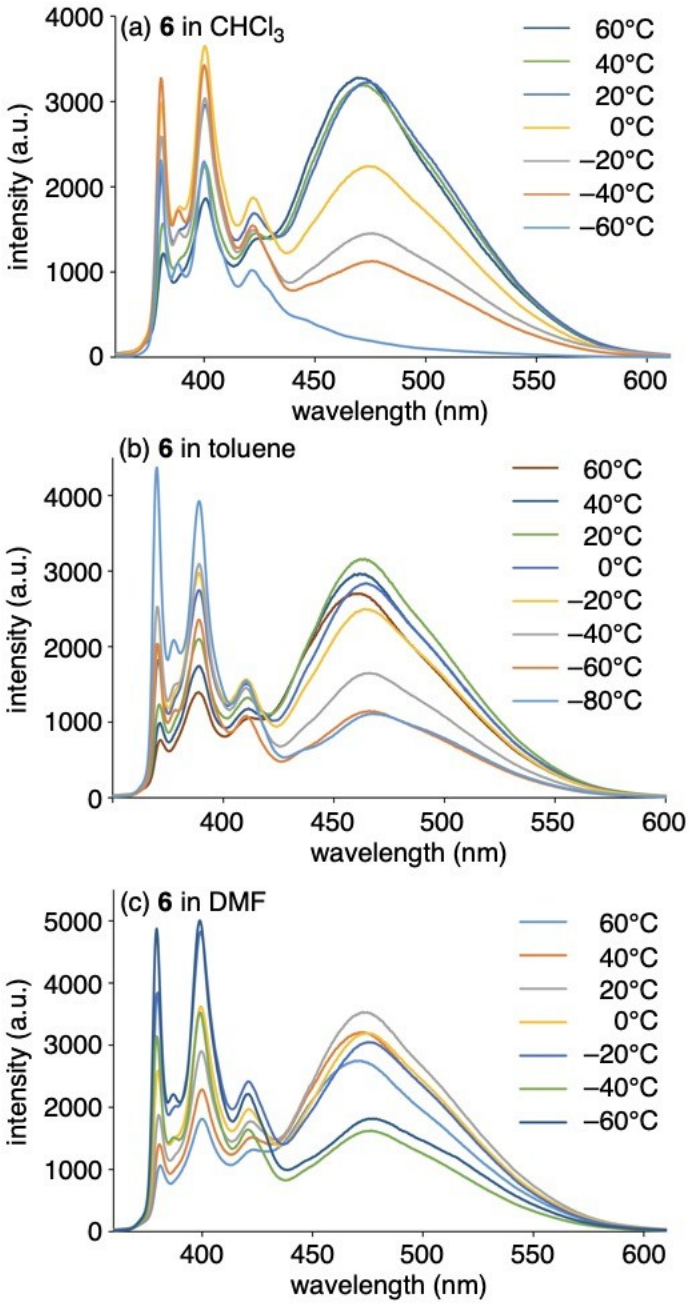

Fig. S29 Variable-temperature fluorescence spectra of **6**, 1.0×10^{-5} M in (a) $CHCl_3$, λ_{ex} = 353 nm, (b) toluene, λ_{ex} = 354 nm, and (c) DMF, λ_{ex} = 352 nm.

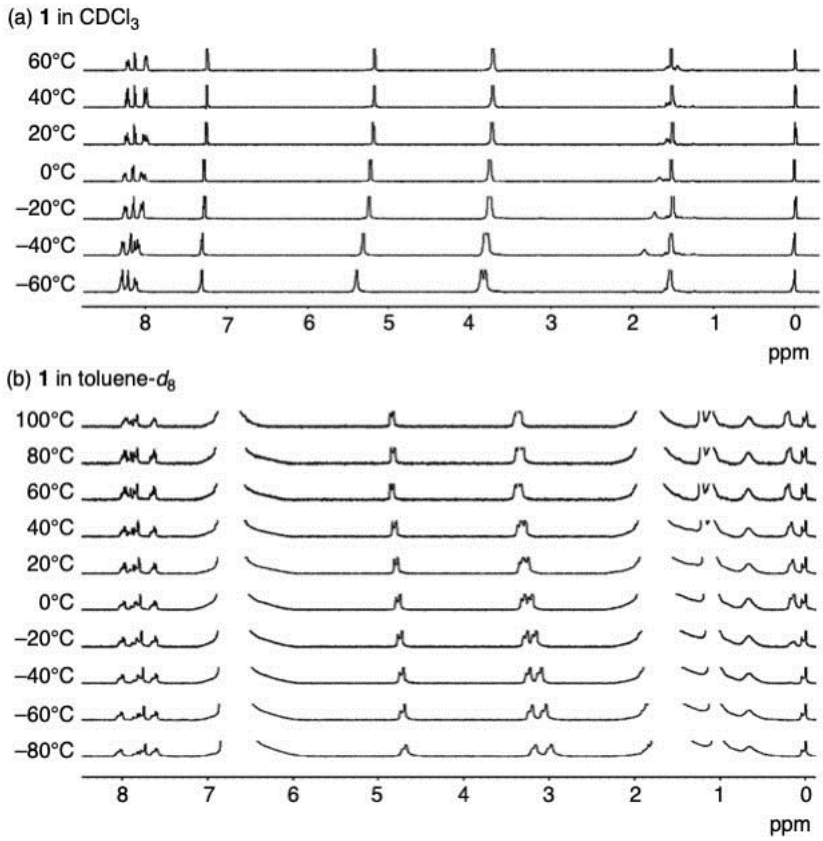

Fig. S30 Variable-temperature ^{1}H NMR spectra (500 MHz) of **1** in (a) $CDCl_3$ and (b) toluene-d_8.

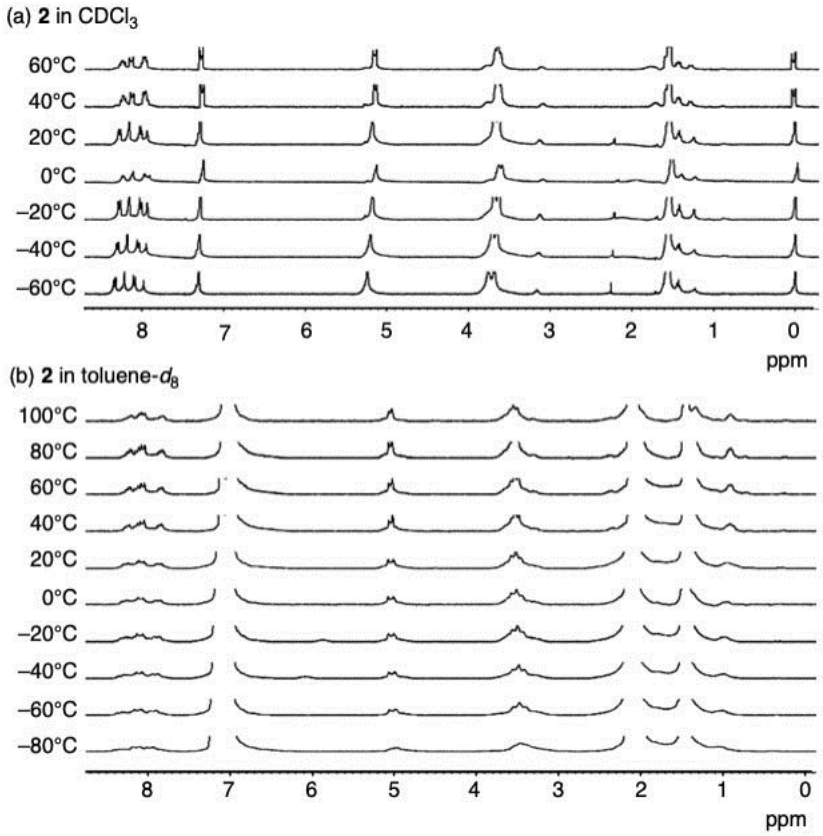

Fig. S31 Variable-temperature ^{1}H NMR spectra (500 MHz) of **2** in (a) $CDCl_3$ and (b) toluene-d_8.

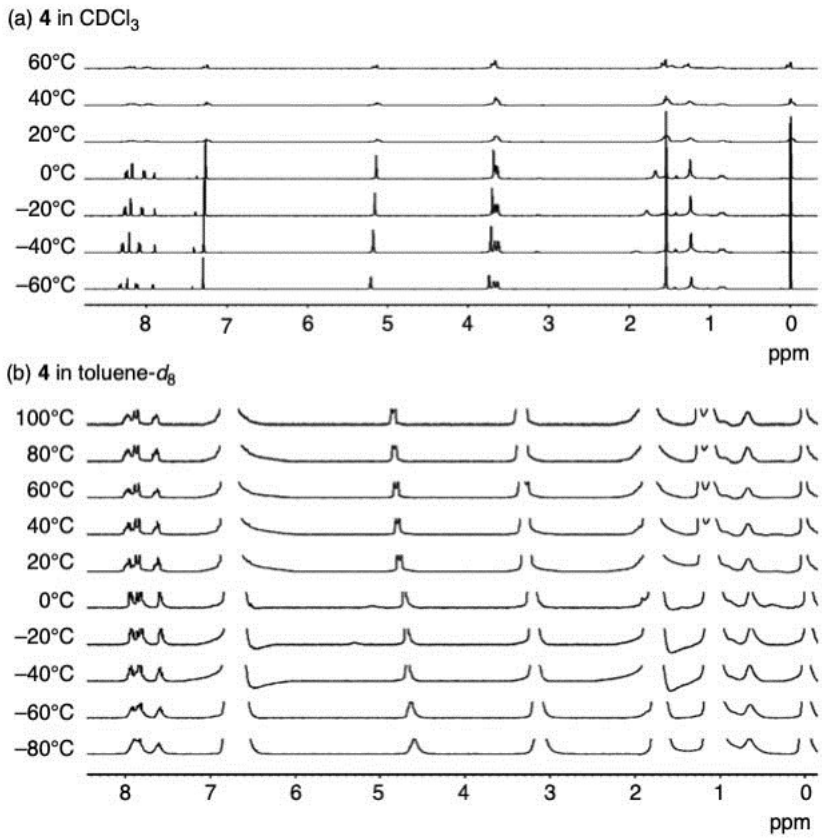

Fig. S32 Variable-temperature ^{1}H NMR spectra (500 MHz) of **4** in (a) $CDCl_3$ and (b) toluene-d_8.

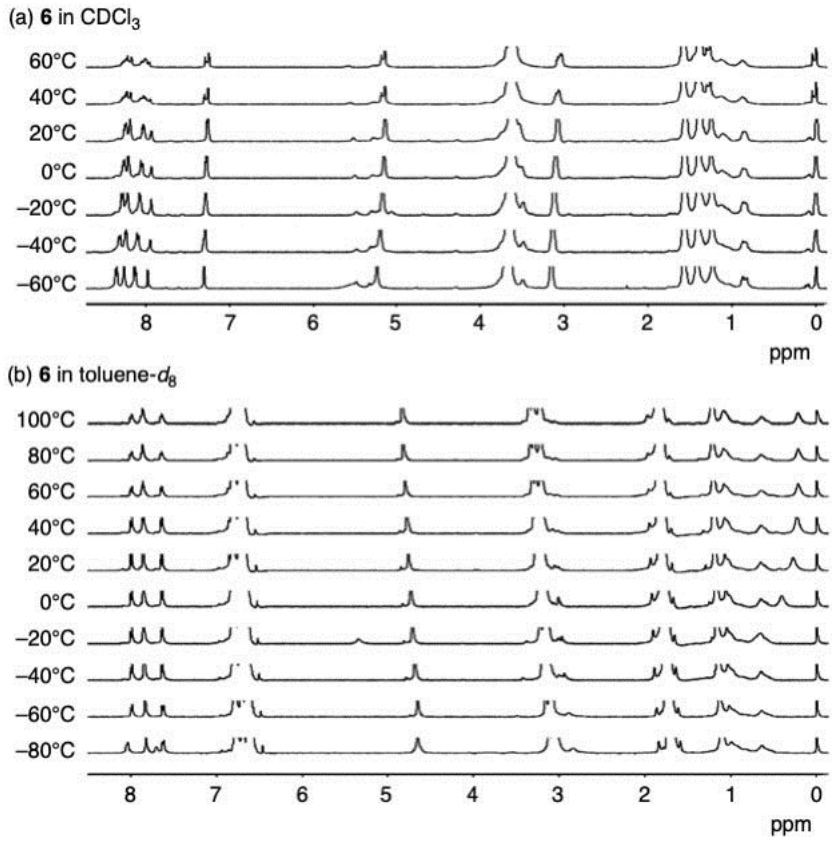

Fig. S33 Variable-temperature ^{1}H NMR spectra (500 MHz) of **6** in (a) $CDCl_3$ and (b) toluene-d_8.

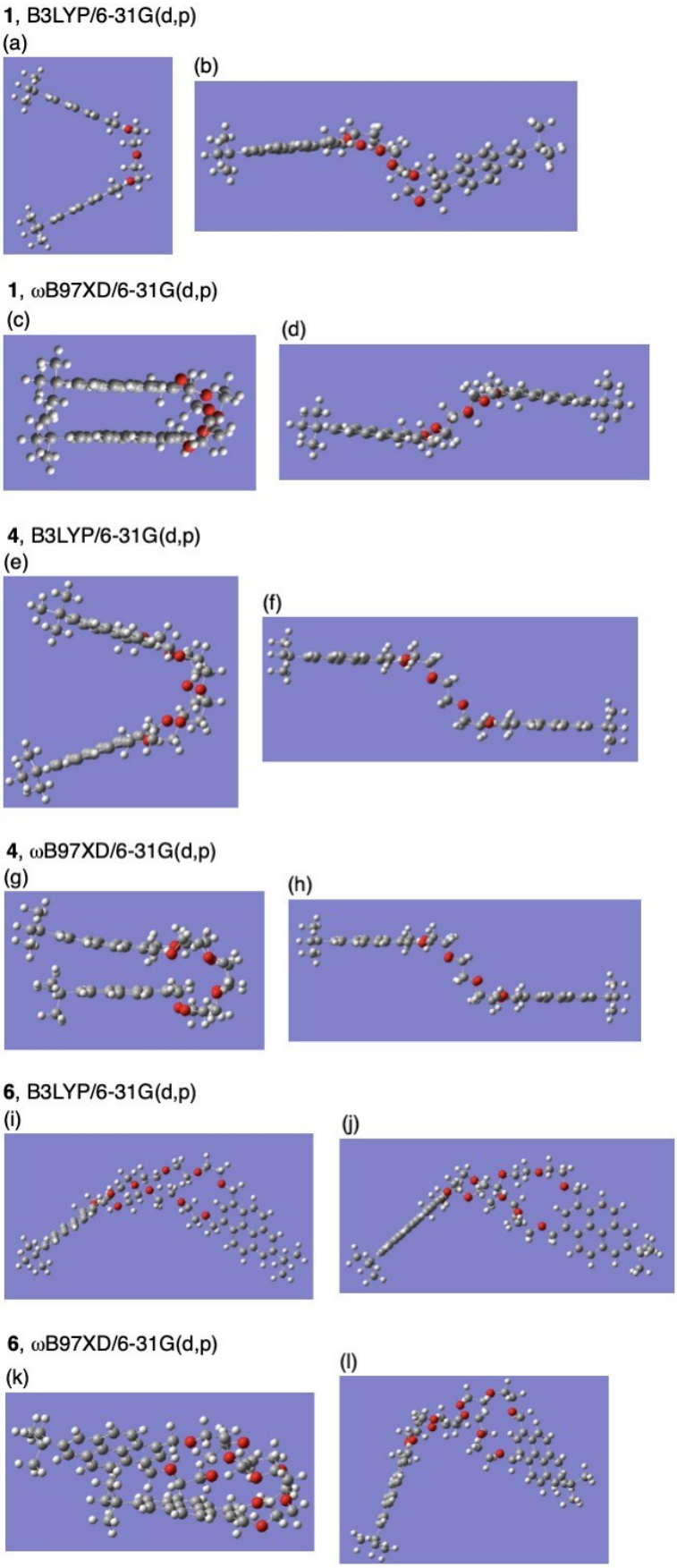

Fig. S34 Optimized conformers of (a)(b)(c)(d) **1**, (e)(f)(g)(h) **4**, and (i)(j)(k)(l) **6**, calculated by using (a)(b)(e)(f)(i)(j) B3LYP/6-31G(d,p) and (c)(d)(g)(h)(k)(l) ωB97XD/6-31G(d,p).

Table S2 Enthalpy and entropy differences of conformers.

compound	B3LYP/3-21G//B3LYP/6-31G(d,p)		ωB97XD/3-21G//ωB97XD/6-31G(d,p)	
	$\Delta\Delta H$(*syn*–*anti*) (kJ/mol)	$\Delta\Delta S$(*syn*–*anti*) (J/mol•K)	$\Delta\Delta H$(*syn*–*anti*) (kJ/mol)	$\Delta\Delta S$(*syn*–*anti*) (J/mol•K)
1	18.2	13.3	–112.7	7.8
4	13.1	10.8	–185.7	–2.9
6	–13.8	13.5	–112.3	4.9